PROBING THE ACTIVE SITE OF PARTICULATE METHANE MONOOXYGENASE: CRYSTALLIZATION OF A NOVEL SAM-TEL/pMMO FUSION PROTEIN

Presented in Partial Fulfillment of the Requirements for *graduation with distinction in Biochemistry* at The Ohio State University

By

Sridevi Ramalingam

*****

ABSTRACT

Particulate methane monooxygenase (pMMO) is an integral membrane metalloenzyme vital for facile methane oxidation in methanotrophic bacteria under ambient conditions. The active site and mechanism of pMMO's conversion of methane to methanol is controversial. Previous research has suggested the existence of a mononuclear copper active site, a dinuclear copper active site, or a mononuclear zinc center based on the crystal structure of the pMMO protein. Conversely, electron paramagnetic resonance (EPR) and X-ray absorption spectroscopies have been used to argue for a trinuclear copper cluster site.

To address the ambiguity surrounding the composition of the active site, we have cloned and overexpressed a SAM-TEL/pMMO peptide fusion protein. This protein consists of a SAM-TEL polymerization domain that is used to promote facile protein crystallization and a 12-residue peptide segment from pMMO that has been proposed to bind the active site trinuclear copper cluster predicted by spectroscopy. Two different versions of SAM-TEL/pMMO protein have been successfully purified and crystallized. SAM1TEL/pMMO fusion protein contains a fused pmoA peptide per SAMTEL monomer and hexagonal crystals of this fusion protein that diffract to a resolution of 2.8 Å have been obtained. SAM3TEL/pMMO fusion protein is composed of one pmoA peptide per three SAMTEL monomers and initial crystallization efforts resulted in small rod-like protein crystals.

Chemical characterization experiments such as UV titration of SAM1TEL/pMMO fusion protein with $Cu(OAc)_2$ support the ability of the pmoA peptide to bind copper. UV titration of a SAM1TEL-control protein reveals that the copper binding ability of the SAM1TEL/pMMO is not a result of the SAMTEL protein. EXAFS experiments further corroborate the ability of the pmoA peptide to bind copper in the proposed ratios (3 copper: 1 peptide) corresponding to that of a trinuclear copper cluster site.

ACKNOWLEDGEMENTS

I would like to express my profound gratitude to my advisor, Dr. Michael Chan, for providing me with the opportunity to pursue research. I am grateful for his support, guidance, and suggestions throughout this research work. I would also like to thank Dr. Marianne Lee without whom this thesis would not be possible. Her encouragement, friendship, and patience in teaching me research methods and etiquette is much appreciated. Finally, I would like to acknowledge Xin Li, and Dr. Manoj Nair for helping me along the way.

LIST OF FIGURES

TABLE OF CONTENTS

CHAPTER 1

INTRODUCTION

Energy is critical for maintaining and improving our quality of life. It is an essential component for the survival of developed countries such as the United States. Currently, fossil fuels (coal, oil, and natural gas) serve as the predominant source of energy in the world, supplying almost 85% of world energy.[1] Of these three non-renewable resources, oil continues to be the world's primary energy source accounting for 36% of world primary energy production.[2]

Automobiles use a majority of the world oil supply. The world consumes approximately 2% of the total oil reserves on the planet per year and the demand for oil is growing at a rate of 1.3 percent per year due to the economic growth of populous nations such as India and China.[3,4] At this rate, world demand for oil will surpass the supply of oil by the year 2016 and deplete this non-renewable resource in the future.[4] The scarcity and the ever-increasing price of oil have led to a renewed interest in developing alternative sources of energy (e.g., methane).

Methane is the most abundant natural gas in the world and is trapped in hydrate cages under the oceans to form methane clathrates.[5,6] These methane hydrate reserves exist in sediments beneath the ocean floor at depths of more than 500 meters where

temperatures are low and pressures are high.[6] Most of these hydrate deposits are found lining the earth's continental margins and in permafrost regions such as Siberia and Alaska.[7]

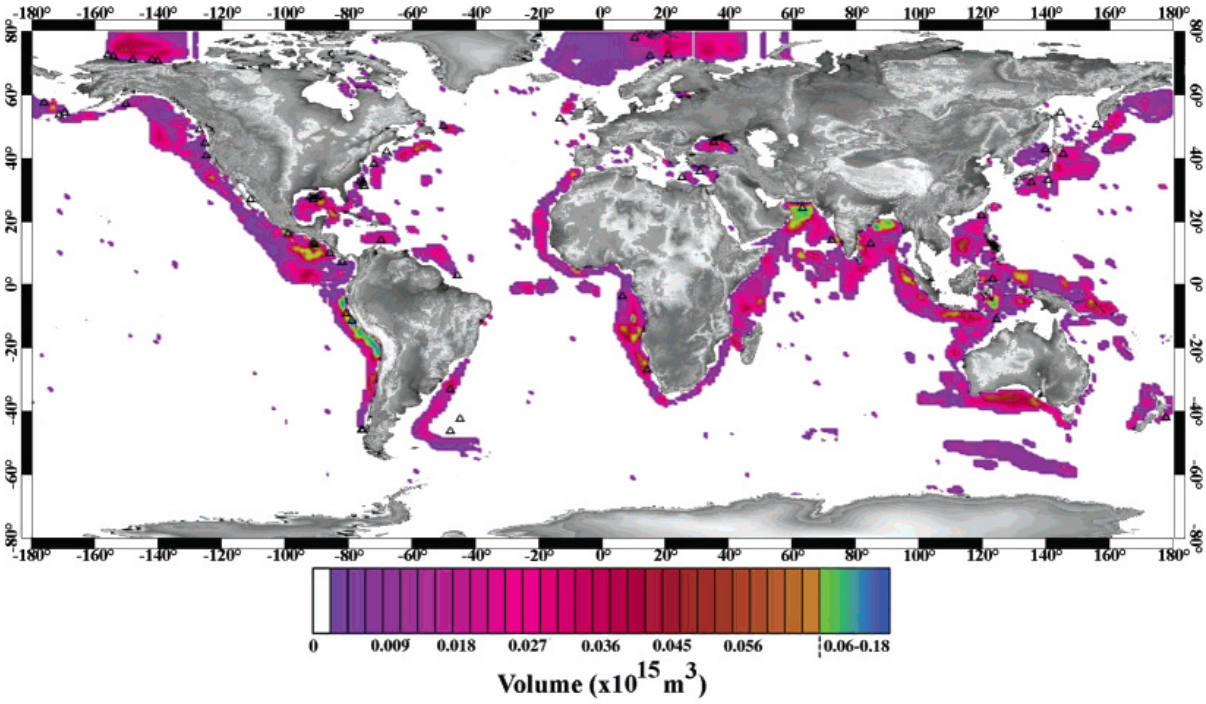

Fig 1.1. Total Volume of Methane from ocean hydrates at STP[7]

There is approximately 4.24 million trillion cubic feet of potential methane gas resources in the ocean methane hydrate reserves.[7] Expanded to standard temperature and pressure (STP), one unit volume of methane hydrate can release over 160 unit volumes of methane gas[8] highlighting the massive amounts of energy potentially available in these hydrate reserves. The current approximation of methane near the earth's continental margins at STP is 1.55 million trillion cubic feet of methane[7] with 6,254 trillion cubic feet in the form of natural gas. In contrast, the world oil reserves total a mere 1,342

billion barrels.[9] Therefore, methane has great promise as the long-term solution to our growing energy needs.

The major challenge in methane's utilization, however, is the fact that it is a gas at ambient temperatures and thus difficult to transport. One potential solution to this challenge is to oxidize the methane to methanol, a liquid fuel at ambient temperatures used in Indy race cars.[10] Unlike the environmental hazards posed by traditional fuels, pure methanol fuel or M100 fuel burns cleaner, reducing hydrocarbon emissions by up to 80% compared with gasoline. M100 fuel also releases only half of the carbon monoxide and approximately an eighth of the nitrogen oxides of gasoline thus reducing the formation of photochemical smog associated with emissions from gasoline powered automobiles.[11]

The chemical conversion of methane to methanol, however, is not simple. Current industrial production of methanol involves an expensive catalytic stream-reforming of methane that requires a large input of energy.[12] The strong carbon-hydrogen bond in methane (104 kcal mol^{-1} C-H bond) makes it difficult to induce the controlled oxidation of methane to methanol and avoid its complete oxidation to CO_2. Given the potential importance of this reaction, many groups have been working to develop an industrial catalyst that can perform the chemical conversion of methane to methanol, but an efficient catalyst has proven difficult to obtain. Fortunately, a potential clue may be provided by a class of enzymes known as methane monooxygenases in methanotrophic bacteria that are capable of promoting this reaction efficiently.

1.1 METHANOTROPHIC BACTERIA

Methanotrophs, a group of gram-negative bacteria found in methane rich environments, function by utilizing methane from the atmosphere as their sole source of carbon and energy. These bacteria contain important metabolic enzymes known as methane monooxygenases (MMO) that catalyze the oxidation of methane and other small hydrocarbons in the presence of oxygen. The first step in the metabolic pathway of these bacteria is the controlled oxidation of methane to methanol by the MMO enzyme. The resulting methanol then undergoes a chemical conversion with the help of another enzyme known as methanol dehydrogenase, to formaldehyde, which is incorporated into organic compounds that supply the bacteria with energy.[13]

There are two forms of methane monooxygenase in methanotrophs: soluble methane monooxygenase (sMMO), found in the cytoplasm of some methanotrophs, responsible for the bioremediation process and the integral membrane metalloenzyme particulate methane monooxygenase (pMMO) found in all methanotrophs.[13] The differential expression of sMMO and pMMO in organisms containing both is driven by the available copper concentration in the growth media. At low copper-to-biomass ratios, sMMO is expressed while pMMO is synthesized at high copper-to-biomass ratio or in copper concentrations greater than 5 μM.[14]

The sMMO system is comprised of three proteins: a hydroxylase (MMOH), a reductase, and a regulatory protein (MMOB), has been studied extensively. The $\alpha_2\beta_2\gamma_2$ structure and the hydroxo-bridged dinuclear iron active site of its hydroxylase (MMOH) has already been determined.[15,16] The particulate methane monooxygenase, on the other hand, is not fully understood despite significant research efforts.

1.2 BASIS FOR A TRINUCLEAR COPPER CLUSTER

Early research into the active site of the pMMO enzyme proved challenging due to the limited methods available to explore the ligand structures of the metal atoms in the enzyme. Electron paramagnetic resonance spectroscopy, Cu K-edge X-ray absorption spectroscopy and the structure determination of this membrane protein are the primary methods available for exploring the composition of its active site.

In 2004, the Sunney I. Chan group utilized spectroscopic methods to annotate the role of the several copper atoms in the functional enzyme. The approximately 15 copper atoms per pMMO protein made straightforward chemical characterization of the copper ions using spectroscopy futile. To study the enzyme using electron paramagnetic resonance (EPR) and Cu K-edge X-ray absorption spectroscopy, some of the fully reduced metal ions in the functional form of the enzyme were oxidized by purifying pMMO under ambient aerobic conditions without its hydrocarbon substrate. Electron paramagnetic resonance spectroscopy (**Fig. 2**) of this partially oxidized form of pMMO, labeled as the "as-isolated" pMMO, led Chan *et al.* (2004) to hypothesize that the active site of the pMMO enzyme is a trinuclear copper cluster site.[17]

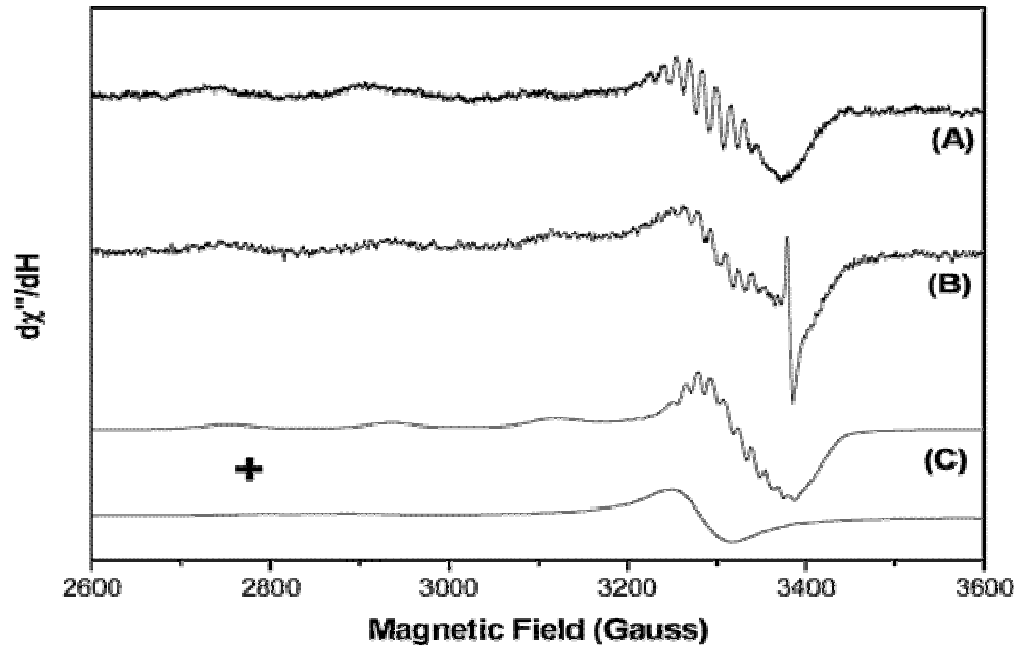

Fig. 1.2. 77 K EPR spectrum of (A) the "as-isolated" pMMO in the purified pMMO-detergent complex, (B) pMMO enriched membranes, and (C) deconvolution of the EPR spectrum to correspond to a type 2 Cu(II) center and a trinuclear Cu(II) cluster.[17]

Though the EPR spectrum of the "as-isolated" pMMO in detergent (A in **Fig. 1.2**) and the pMMO enriched membranes (B in **Fig. 1.2**) both resemble a type 2 Cu(II) center, Chan *et al.* resolved this signal as the sum of two EPR signals; one from a type 2 Cu(II) center and the other from a trinuclear Cu(II) cluster. These EPR results were also corroborated by Cu K-edge X-ray absorption spectroscopy experiments conducted using the "as-isolated" pMMO by Nguyen *et al.* The "as-isolated" form of pMMO by Nguyen *et al.* was produced by incubating the fully reduced form of the pMMO enzyme in dioxygen for distinct periods of time. The Cu K-edge absorption spectrum of these various "as-isolated" forms of pMMO revealed that no more than 30-40% of the copper atoms, or approximately 6 copper atoms, in the enzyme were oxidized at one time.[18] Based on these observations, the Sunney I. Chan group proposed that the approximately

15 copper atoms per pMMO enzyme were divided into two different clusters: two catalytic trinuclear copper clusters or C-clusters comprised of 6 copper atoms and three electron transfer trinuclear copper clusters or E-clusters totaling 9 copper atoms.[18]

The two C-clusters are suggested by Chan *et al.* to participate in dioxygen and hydroxylation chemistry while the three E-clusters are thought to facilitate electron transfer to re-reduce the C-clusters during turnover. EXAFS experiments using acetylene as a suicide substrate indicated that although both C-clusters reacted with dioxygen, only one C-cluster was directly involved in the alkane hydroxylation.

With this knowledge, the Chan lab proposed a scheme to explain the EPR spectrum of the "as-isolated" pMMO that results in one type 2 Cu(II) signal and another trinuclear Cu(II) cluster signal. In this scheme, **Fig. 1.3**, the two C-clusters labeled "**A**" and "**B**" are activated by dioxygen to form the Cu(II) mixed valence bis(μ-oxo)$Cu^{II}Cu^{III}$ tricopper core necessary for facile oxo transfer chemistry. Following this, there is an electron transfer from one cluster (cluster "**A**") to the other (cluster "**B**") in order to complete the dioxygen chemistry at the latter C-cluster site (cluster "**B**"). Chan *et al.* argue that if this electron transfer occurs prior to the hydroxylation of the substrate, the facile oxo transfer chemistry is aborted and the reaction would culminate in the formation of a trinuclear copper cluster site at C-cluster "**B**" and a type 2 Cu(II) center at C-cluster "**A**". In the presence of a hydrocarbon substrate such as methane, used in **Fig. 1.4.**, the hydroxylation chemistry coupled with the dioxygen chemistry leads to the formation of the trinuclear copper cluster at both C-cluster "**A**" and C-cluster "**B**" thus resulting in the EPR signal consistent with that of only the trinuclear copper cluster.[17]

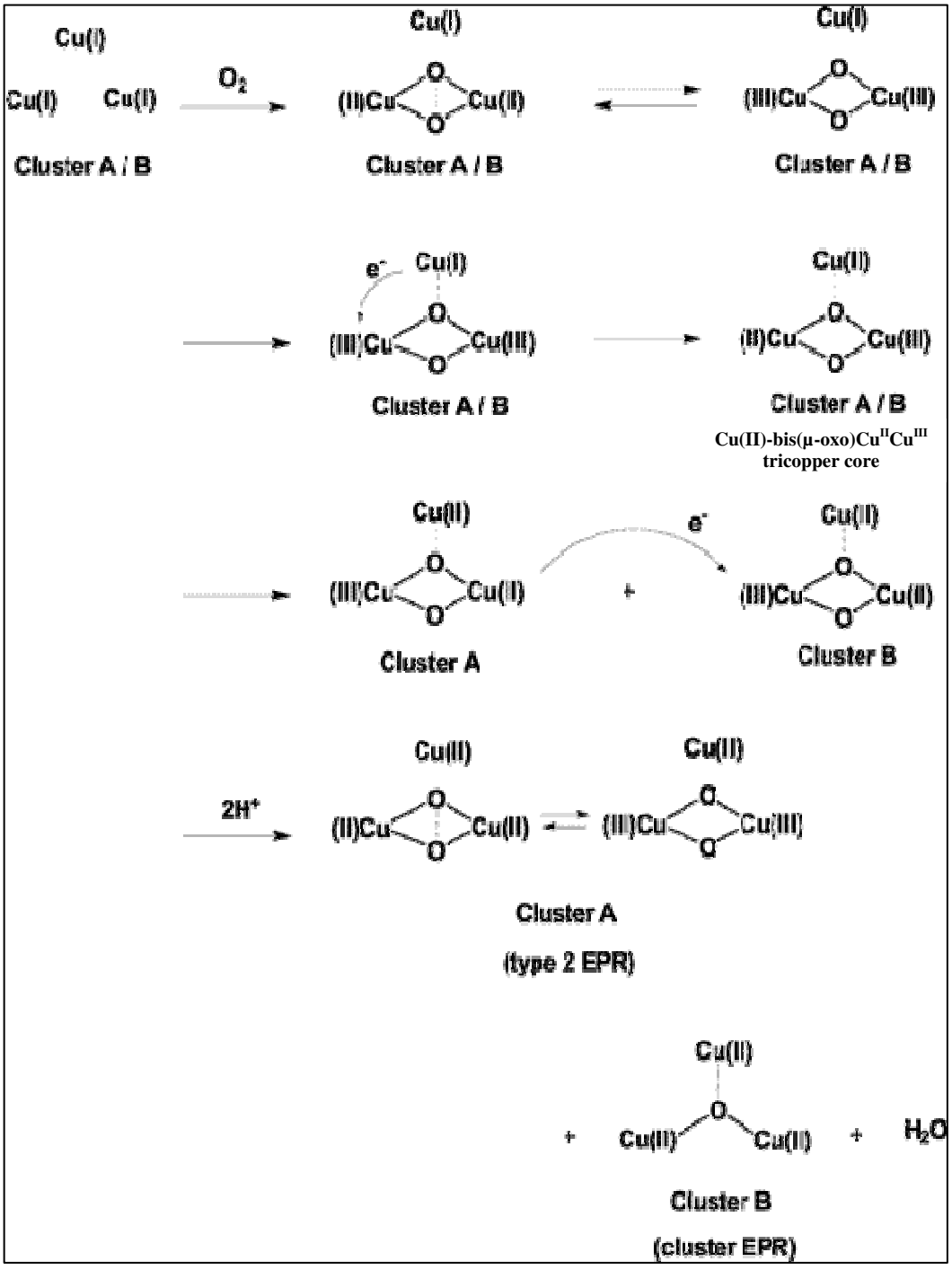

Fig. 1.3. Scheme explaining the EPR results of the "as-isolated" pMMO.[17]

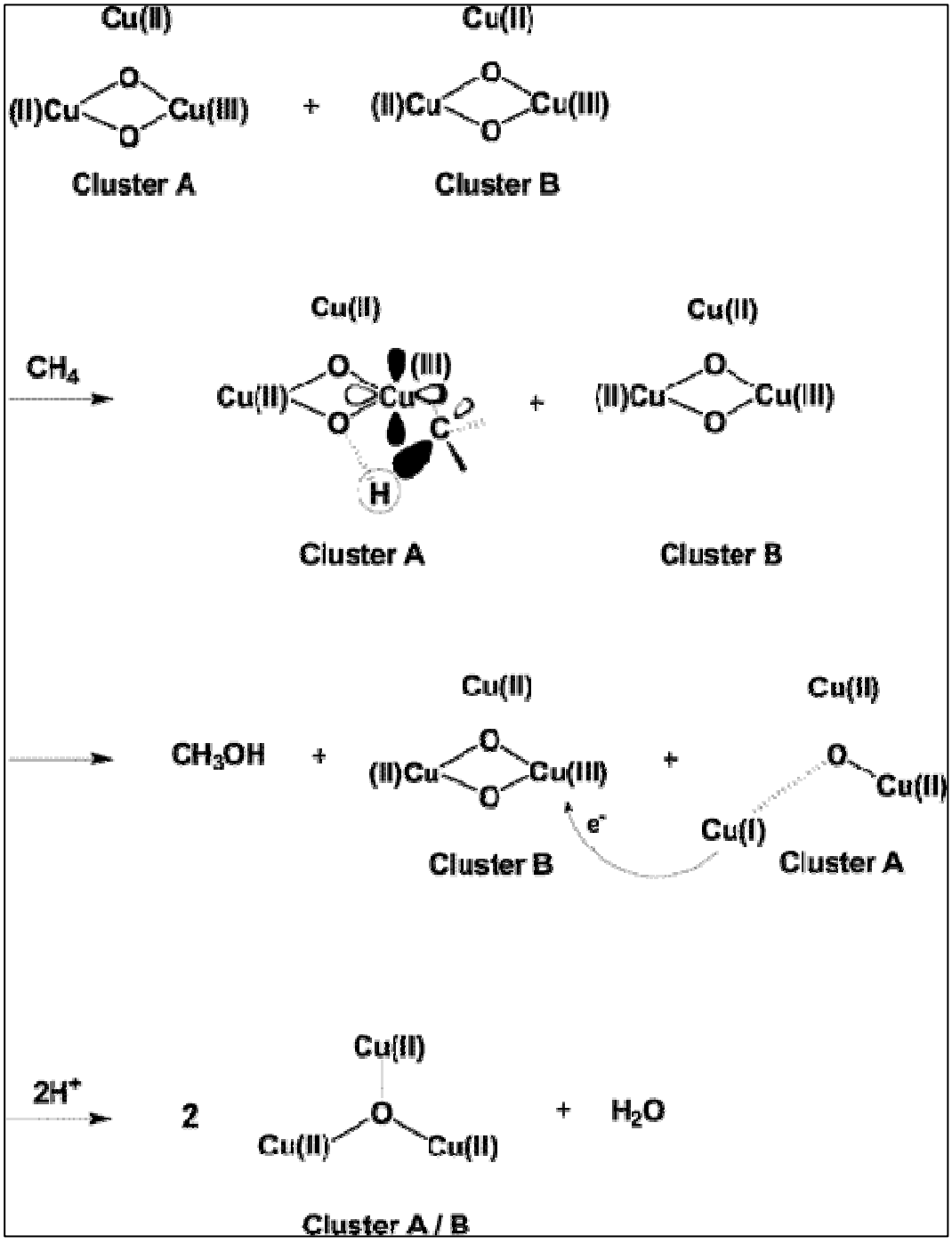

Fig. 1.4. Scheme representing the physiological hydroxylation function of the pMMO enzyme.[17]

1.3 MECHANISM OF A TRINUCLEAR COPPER CLUSTER

The possible mechanism of hydroxylation chemistry using the trinuclear copper cluster by the pMMO enzyme has also been proposed by the S.I. Chan group.[17] The singlet "oxene" insertion mechanism consists of an active oxene being delivered side on from the dioxygen activated Cu(II) mixed valence bis(μ-oxo)$Cu^{II}Cu^{III}$ tricopper species. This process is dictated by the "conservation of spin multiplicity" where the odd electron (↑) of the oxygen in the transition state pairs with the antiparallel spin of the electron (↓) on the carbon in the transition state. Likewise, the odd spin of the electron (↓) from the oxygen in the transition state pairs with the antiparallel spin electron (↑) of the hydrogen in the transition state. Since the two spins of the respective electrons are already favorably aligned and therefore do not need to undergo spin crossover, the C-O and the O-H bond formations are quick and efficient.[19] The pairing of electrons and the structure of the transition state is shown in **Fig. 1.5.** The rapid bond formations which take place in no more than 10 femtoseconds prevent the inversion of configuration of the carbon center that is hydroxylated in this process. This is consistent with the hydroxylation chemistry mediated by the pMMO enzyme where the hydrocarbon substrate retains its configuration.[17]

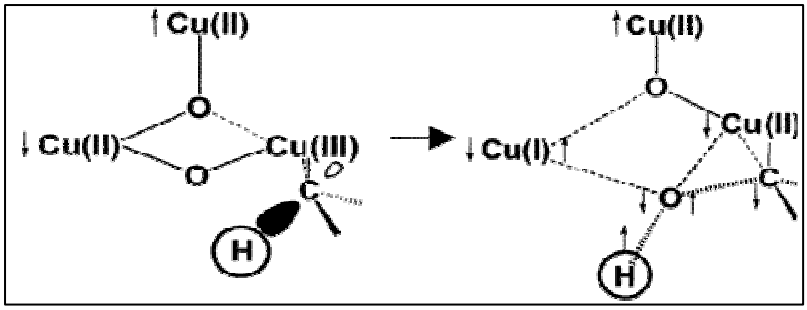

Fig. 1.5. Singlet "oxene" mechanism from the Cu(II) mixed valence bis(μ-oxo)$Cu^{II}Cu^{III}$ tricopper species to methane to the transition state. ↑ and ↓ arrows denote "up" and "down" directions respectively of the unpaired electrons.[17]

Therefore, based on EPR experiments and the predicted mechanism of the trinuclear copper cluster to facilitate facile oxygen insertion in a C-H bond, the Sunney I. Chan group proposed early on that the hydroxylating C-cluster or the active site of pMMO is a trinuclear copper cluster. However, this hypothesis could not be corroborated without the structure of the particulate methane monooxygenase.

1.4 CRYSTAL STRUCTURE OF PARTICULATE METHANE MONOOXYGENASE

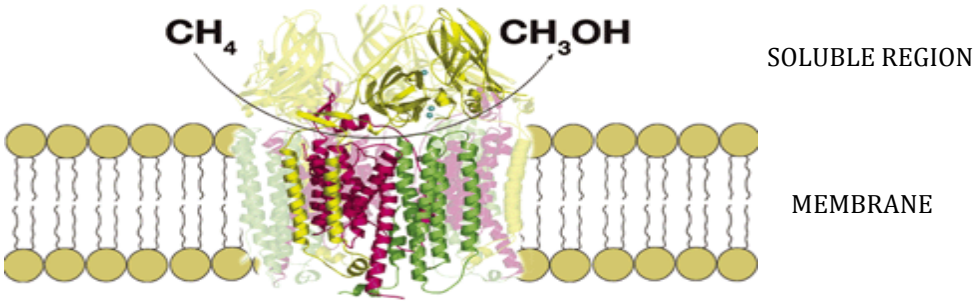

Fig. 1.6. Model of pMMO in membrane bilayer. [21]

A breakthrough in the study of pMMO occurred in 2005 with the structure determination of *Methylococcus capsulatus* (Bath) pMMO by Amy Rosenzweig and Rachel Lieberman. The 2.8 Å enzyme structure reveals three copies of three subunits each: pmoA, pmoB, and pmoC , forming a cylindrical $\alpha_3\beta_3\gamma_3$ trimer. The soluble portion of the metalloenzyme is derived from the pmoB subunit while the pmoA and the pmoC subunits primarily reside in the membrane.[20] Unfortunately, the structure still leaves the active site and the mechanism of the enzyme ambiguous.

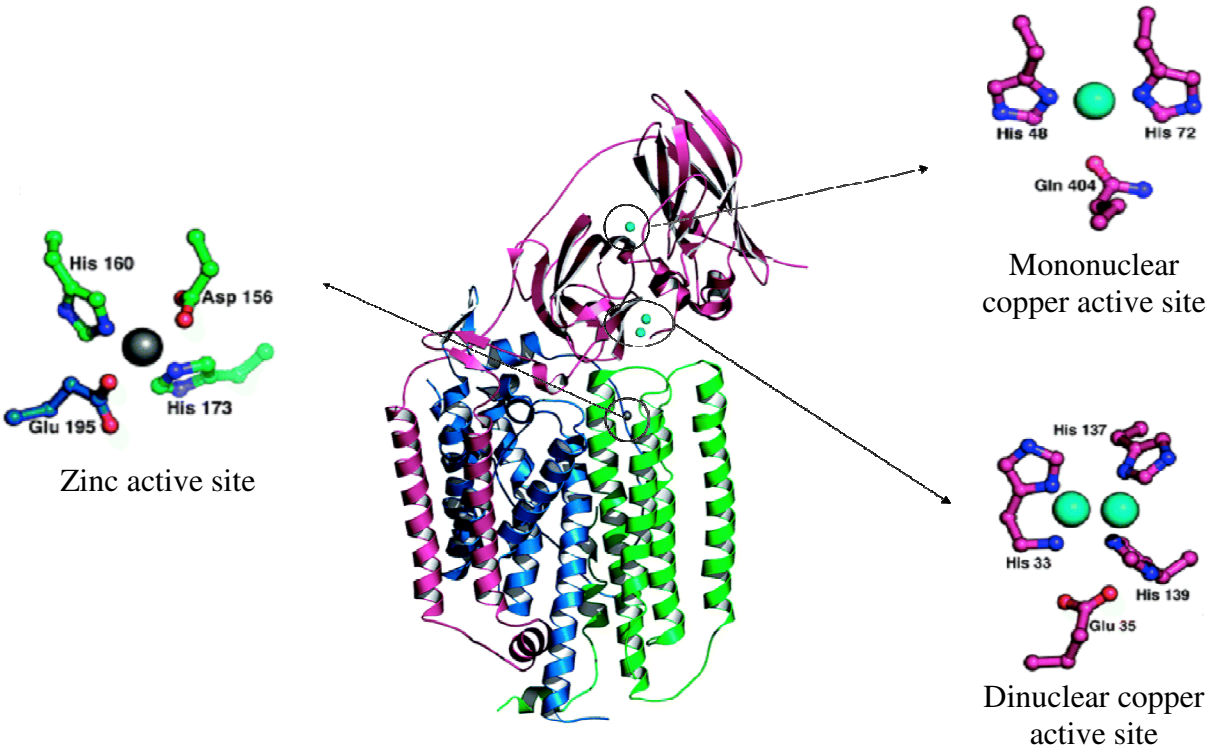

Fig. 1.7. One of the three protomers of pMMO with subunits pmoA, pmoB, and pmoC shown in blue, magenta, and green respectively. Copper ions are represented as green spheres and a zinc ion as a gray sphere.[21]

The crystal structure shows three metal centers present per protomer that, argued by Rosenzweig *et al.*, could serve as the active site of the pMMO enzyme. The first metal center is located in the soluble region of the enzyme approximately 25 Å above the membrane. This metal center was assigned as a mononuclear copper ion based on peaks in anomalous Fourier maps corresponding to copper. The mononuclear copper active site is shown to coordinate with the δ nitrogen atoms of His 48 and His 72 with Gln 404 nearby. The possibility of this mononuclear copper site as the active site of pMMO arises from the hydroxylation ability of mononuclear copper centers in other enzymes such as peptidylglycine α-hydroxylating monooxygenase (PHM) and dopamine β-monooxygenase (DβM). The copper site in these enzymes is ligated by two histidines and

a vital methionine residue necessary for enzyme reactivity. The mononuclear copper site proposed by Rosenzweig and Liebermann however does not contain this essential methionine residue.[20,21]

The second metal site is approximately 10 Å above the membrane and approximately 21 Å from the mononuclear copper site. This site was characterized by Rosenzweig and Lieberman as a dinuclear copper site based on two distinct peaks observed in the anomalous Fourier map. One copper ion in this dinuclear site is coordinated by His 33 that is held in position by hydrogen bonds with Glu 35 while the second copper ion is shown to be coordinated by the δ nitrogen of His 137 and the ε nitrogen of His 139. This dinuclear copper site is argued by Rosenzweig and Liebermann as the most attractive possibility for the active site out of the three metal centers. The authors refer to dicopper centers in tyrosinase and other proteins capable of binding and/or activating dioxygen for oxidation. Rosenzweig and Lieberman also indicate that the dinuclear copper site may function in electron transfer due to its structural similarities with cytochrom *c* oxidase subunit II rather than as the catalytic site.[20,21]

Lastly, the third metal center is located in the membrane approximately 19 Å away from the dinuclear copper site and is characterized as a zinc ion based on peaks in a zinc anomalous Fourier map. The coordination of the zinc ion involves Asp 156, His 160 and His 173 from the pmoC subunit and a tentative Glu 195 from pmoA. However, the likelihood of a zinc active site is decreased due to the low zinc content in the pMMO protein; measured to be less than 0.2 moles of zinc per 100 kDa. The presence of Zinc in the crystal structure is noted to be from the Zinc acetate in the crystallization buffer.[20]

1.5 SUPPORT FOR TRINCULEAR CLUSTER DESPITE pMMO CRYSTAL STRUCTURE

The overall pMMO crystal structure detailed above does not display any metal sites consistent with that of a trinuclear copper cluster site argued for by the Sunney Chan group. However, the 3-4 copper ions seen in the crystal structure do not account for the number or the type of Cu(II) signals observed by EPR nor do they agree with the approximately 15-17 copper atoms noted by Nguyen *et al.*[18], Yu *et a.l*[22], and Xin *et al.*[23] for a fully functional pMMO enzyme. A recent repeat of the purification procedures for pMMO utilized by Rosenzweig *et al.* revealed that as many as 12 out of the approximately 15 copper atoms were lost following ammonium sulfate fractionation. Thus, it comes as no surprise that the Rosenzweig pMMO structure was reported to be of an inactive form of the pMMO enzyme, suggesting that the metal atoms responsible for the enzyme's activity are lost during the harsh purification conditions.

Furthermore, the two copper sites seen in the crystal structure exist in the soluble region of the enzyme where their interactions with nonpolar substrates like methane are limited. In order for methane and other short hydrocarbon substrates to access the mononuclear and the dinuclear copper sites highlighted by Rosenzweig, a tight hydrophobic pocket must exist near the two sites to accommodate the travel of the substrate.[24] The crystal structure of pMMO revealed no such hydrophobic pocket near these two supposed copper active sites. Therefore, the possibility of a trinuclear copper cluster as the active site of the pMMO enzyme cannot be dismissed.

To garner more support for the existence of the trinuclear copper cluster in the pMMO enzyme, Dr. Michael K. Chan of The Ohio State University worked with the S.I.

Chan group to identify a site within the pMMO enzyme that might harbor this theoretical trinuclear copper cluster site. They identified one such site within the pmoA subunit (site D in **Fig. 1.8.**) which contains several liganding residues such as His38, Met42, Met45, Asp47, Trp48, Asp49, and Glu100 from pmoA subunit and Glu154 from pmoC subunit necessary to bind and localize the copper atoms. The S.I. Chan group (2007) believe that these hydrophilic residues previously discarded as a metal binding site should have counterions such as copper atoms to balance the high charge in this cluster. In support of this view, when a fully oxidized tricopper cluster was modeled into site D in **Fig. 1.9.** the computed electrostatic energy of the protein was found to be significantly reduced.[25]

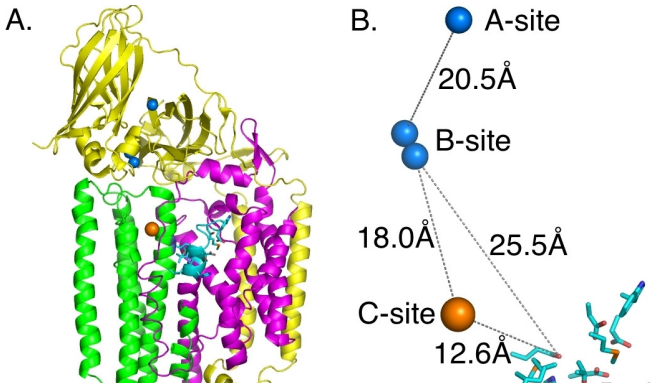

Fig. 1.8. Structure of pMMO highlighting potential site for trinuclear copper cluster. (A) Ribbon diagram, (B) Figure showing clusters in crystal structure plus D-site, which is the proposed trinuclear copper site.[25]

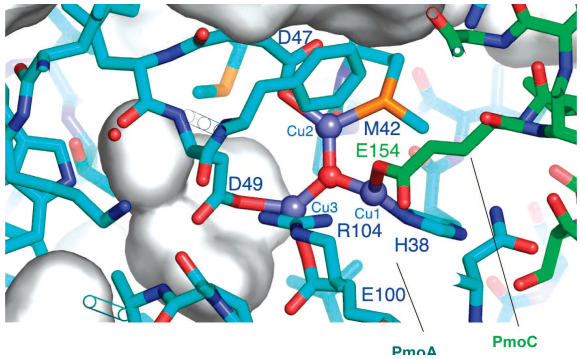

Fig. 1.9. Image detailing the peptide interactions with a modeled trinuclear copper cluster in proposed pMMO active site D.[25]

Another notable aspect of active site D shown in **Fig. 1.9.** is its location in the membrane portion of the pMMO enzyme. Also, there exists a hydrophobic pocket near site D that is long enough to bind only C1-C5 straight chain hydrocarbons. Analysis of this hydrophobic pocket by Chan *et al.* (2008) found that pentane, the largest hydrocarbon capable of being hydroxylated by the pMMO enzyme, could be successfully fitted into this hydrophobic pocket and positioned in the proper orientation to yield the correct stereochemical product (**Fig. 1.10**).[26]

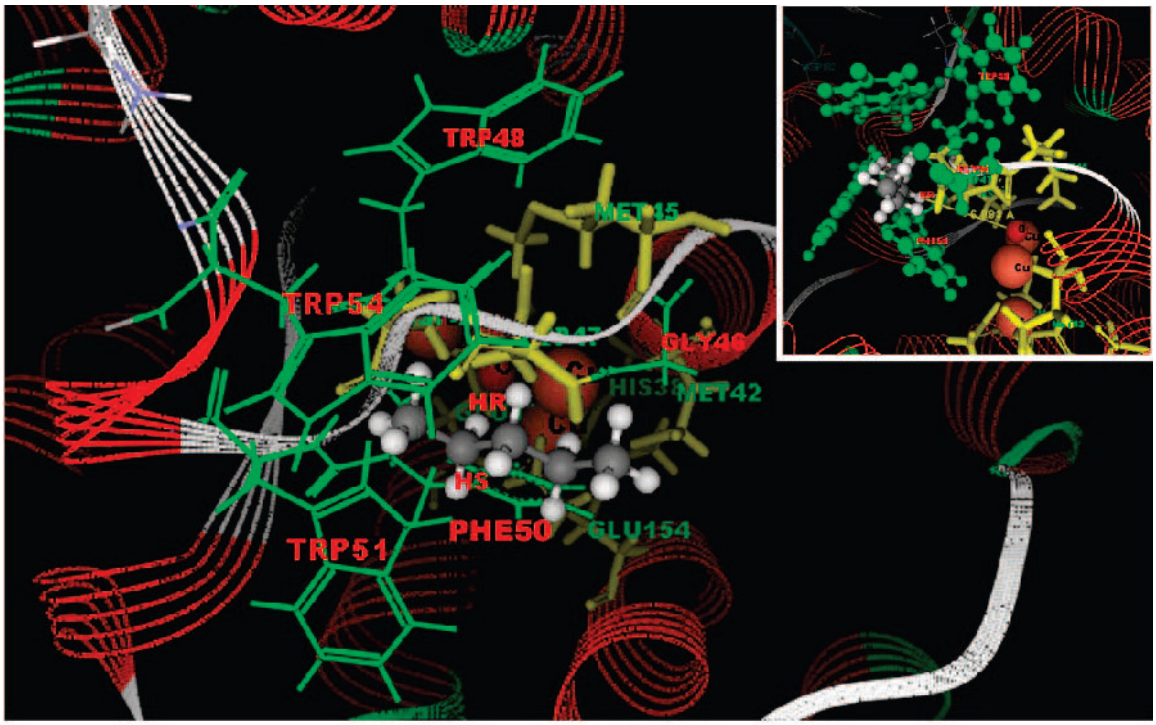

Fig. 1.10. Modeling of pentane in the hydrophobic pocket consisting of aromatic residues Trp48, Phe50, Trp51, and Trp54 of pmoA subunit near site D.[26]

An important characteristic of the proposed active site D is that much of the ligating residues of this site are from a short peptide within the pmoA subunit of the pMMO enzyme (**Fig. 1.11**). This feature opens up the possibility of its synthesis and subsequent analysis and structure determination. To test this idea, the Steve F. Yu group

(Academia Sinica) synthesized the pmoA(38-49) peptide, HIQAMLTMGDWD, and provided it to the S.I. Chan group for characterization. Preliminary studies revealed that the ligating residues could bind copper at the proposed ratios corresponding to a trinuclear copper cluster.

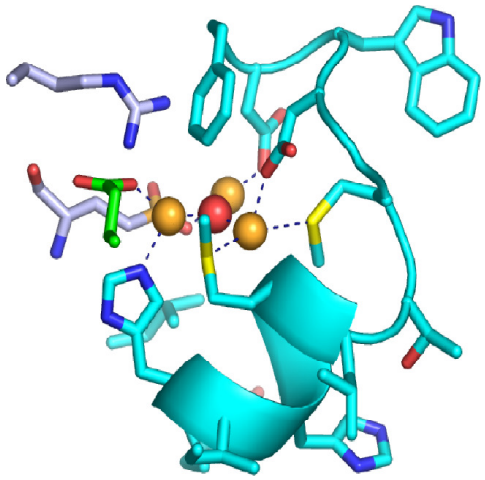

Fig. 1.11. Model of the trinuclear copper cluster in pMMO displaying that many of its ligating residues come from a short peptide

UV absorption experiments where the pmoA peptide was titrated with $Cu(OAc)_2$ showed cooperative binding of copper by the pmoA peptide. The maximum UV absorbance was achieved at a Cu:pmoA peptide ratio of 3:1 exhibiting the peptide's ability to bind 3 copper atoms similar to that of a trinuclear copper cluster. EPR experiments conducted by the S.I. Chan group also supported the UV titration results. EPR spectra of the pmoA peptide with less than 3 eq. of copper displayed similar characteristics to that of the trinuclear copper cluster signal while more copper equivalents produced a signal resembling a Type 2 Cu(II) center.

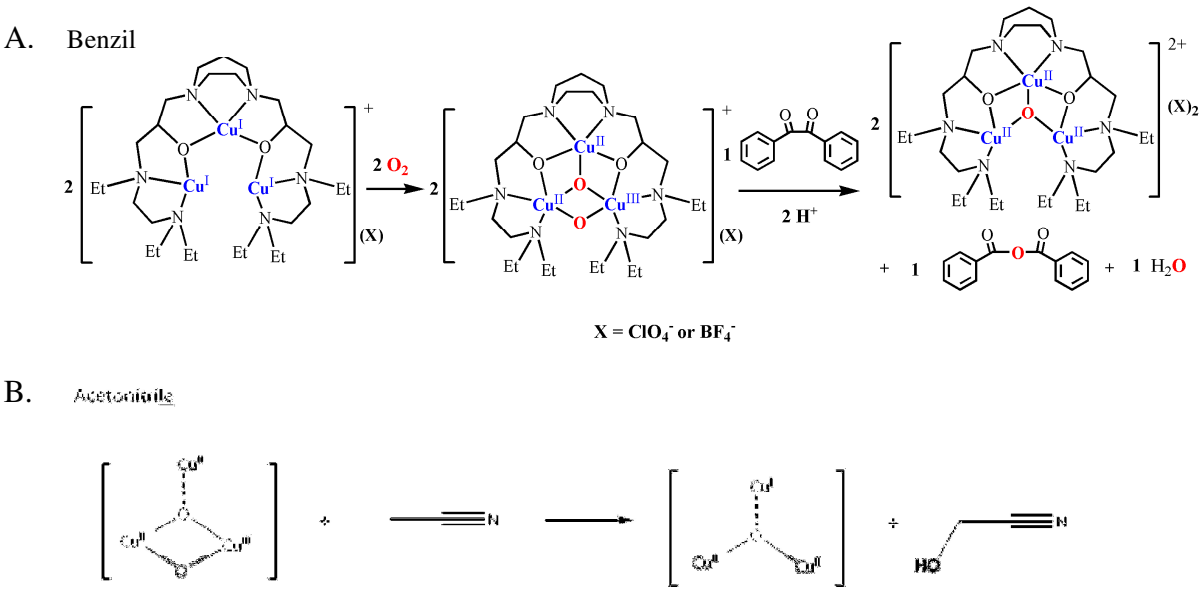

Fig. 1.12. (A) Reaction of the trinuclear copper cluster, $[Cu^{I}Cu^{I}Cu^{I}(L)]$ with dioxygen resulting in an intermediate bis(μ_3-oxo)trinuclear copper(II, II, III) species that mediates facile "singlet oxene" insertion into a C-C bond of benzyl, (B) Facile "singlet oxene" insertion into a C-H bond of acetonitrile mediated by the bis(μ_3-oxo)trinuclear copper(II, II, III) intermediate species.[27]

Further support that the active site of pMMO might be a trinuclear copper cluster came from biomimetic model studies reported by the S.I. Chan laboratory in 2007. They were able to prepare a set of trinuclear copper cluster model complexes bound to the ligands 3,3'-(1,4-diazepane-1,4-diyl)bis(1-((2(dimethyl-amino)ethyl)(methyl)amino) propan-2-ol) (**7-Me)** or 3,3'-(1,4-diazepane-1,4-diyl)bis(1-((2(dimethyl-amino)ethyl) (ethyl)amino)propan-2-ol) (**7-Et)** that exhibited hydroxylation capability. These tricopper complexes reacted with dioxygen to form the intermediate bis(μ_3-oxo)trinuclear copper(II, II, III) species capable of facile oxygen atom insertion into C-C bond of benzil and C-H bond of acetonitrile.[27] Though the substrates used here are not straight chain hydrocarbons, the experiments verify the ability of a trinuclear copper cluster in mediating facile oxygen transfer.

CHAPTER 2

The promise of this pmoA(38-49) peptide to bind a trinuclear copper cluster led to the Michael K. Chan lab's interest in the crystallization and the subsequent structural determination of the copper bound pmoA(38-49) peptide.

2.1 SIGNIFICANCE

The structural characterization of this proposed active site peptide can lead to several applications in the future. The facile conversion of methane to methanol mediated by the pMMO enzyme would be a cornerstone for a viable methanol economy, a concept that has been proposed by many, including the Nobel Laureate George Olah[30], as an alternative to the ethanol and the hydrogen economy. Methanol was previously mandated as a fuel for cars in the Indianapolis 500 and continues to play a role in other energy demands. Solving the structure of the copper cluster site could aid in our understanding the mechanism by which the conversion takes place in methanotrophic bacteria. This could lead to a new, more efficient production of methanol that could then be implemented as fuel in automobiles, thus achieving a major step forward in our goal of energy independence.

Also, the uses of methanol extend far beyond transportation fuel. Several goods such as plastics, antifreeze, silicones, explosives and even textiles use methanol as their basis for production[8]. Elucidating the mechanism by which methanotrophic bacteria convert methane to methanol aided by structural analysis may very well reduce the cost of methanol-derived products in the global market.

Moreover, the structure determination of the copper bound pmoA peptide can accelerate the development of oxidation catalysts capable of oxidizing not just methane but also other hydrocarbons.

2.2 STRATEGY

The ultimate goal of the research endeavor undertaken by myself and Marianne Lee requires the crystallization of a small target peptide (HIQAMLTMGDWD) bound to copper ions. This presents with its own set of challenges. The relative instability of small peptides marked by the lower percentage of interactions between their residues make them difficult to crystallize. To tackle this problem, our idea was to fuse the target pmoA peptide to the C-terminus of a SAM domain of the proto-oncogene TEL (Translocation, Ets, Leukemia).

TEL (Translocation, Ets, Leukemia) is a transcriptional repressor containing a sterile alpha motif or SAM domain that has the ability to polymerize. *In vivo*, the SAMTEL domain forms a left-handed helical polymer with six subunits per turn. This polymerization characteristic makes the wild-type SAMTEL protein difficult to overexpress and purify as it oligomerizes and becomes insoluble.[28] To overcome the solubility problems precluding the structure determination of the SAMTEL protein, the James Bowie lab at UCLA screened for various mutants containing mutations at the module interfaces that induce pH dependent polymerization.[29] One such mutation identified by the Bowie lab is the V80E mutation that renders the SAMTEL soluble at pH above 7.0. Using this soluble SAMTEL V80E mutant, the Bowie lab explored the use of this protein as a crystallization tool. The design of this crystallization tool consists of two

SAMTEL domains, an N-terminus V80E SAMTEL mutant and a C-terminus wild-type SAMTEL that are connected by a linker consisting of Gly_4Ser repeats. This 2TEL module was fused to several different proteins with the hope that the polymeric backbone formed from strong crystal contacts would facilitate crystallization. Nauli *et al.* report the successful crystallization of eleven of these 2TEL fusion proteins including the crystallization of the Zn-binding domain of the human polyhomeotic protein (hPhZn) and the C-terminal domain of the human RING2 protein (hRING2) that proved difficult to crystallize on their own. The crystals of the 2TEL-hRING2 diffraction to a resolution of 2.3 Å but the data could not be used for structure determination due to the high mosaicity or disordered packing of the fusion protein molecules in the crystal.[29]

Nauli *et al.* also found that the 2TEL module's ability to crystallize is not severely compromised in the presence of detergents meaning that this fusion method may also be useful for the crystallization of membrane proteins. In any case, the 2TEL module served as an efficient crystallization tool promoting the crystallization of different sized proteins. The Bowie lab therefore created SAMTEL constructs with varying linker sequence and several unique restriction sites for the introduction of new DNA sequences for the purpose of crystallizing SAMTEL fusion proteins.[29]

Fig. 2.1. Diagram detailing the research strategy for the structure determination of pmoA(38-49) peptide

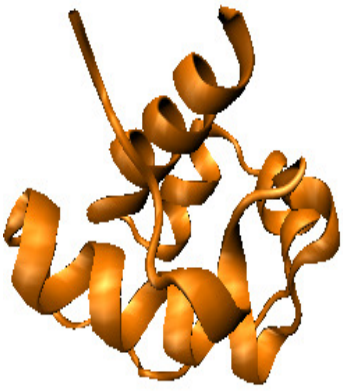

Structure of SAM-TEL monomer

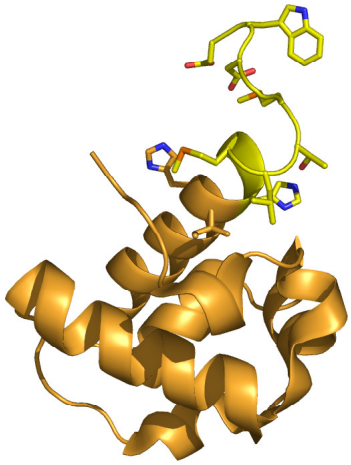

Model of SAM-TEL/pMMO fusion protein with SAMTEL colored in orange, and pmoA(38-49) peptide in yellow

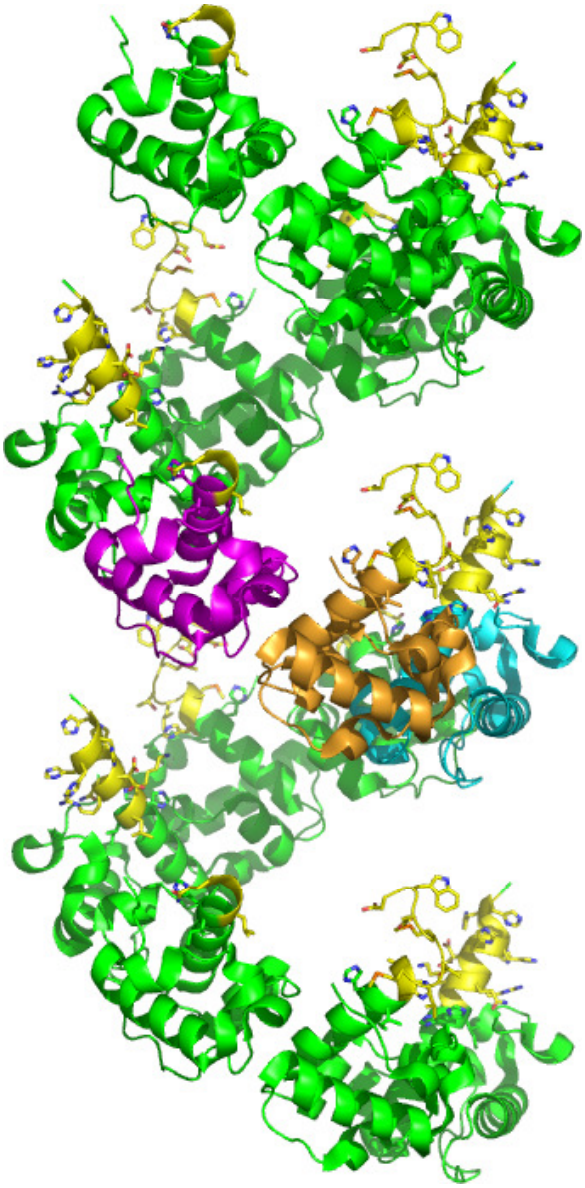

Predicted SAM-TEL/pMMO polymer

Relating this to our project of the structure determination of the pmoA(38-49) peptide, the premise is to exploit the ability of the SAMTEL V80E mutant to form a repeating polymer in order to facilitate crystallization; only this time, instead of proteins, we apply this strategy to a small peptide. The notion to form this SAM-TEL/pMMO fusion protein is aided by the fact that the end residues of the SAMTEL C-terminal helix as well as the beginning residues of the pmoA peptide are both His-Leu. This ensures that the pmoA peptide will anchor tightly to the C-terminus of the SAMTEL and avoid the structural disorder witnessed in the 2TEL-hRING2 fusion protein.

Although concerns relating to the influence of the larger SAMTEL protein on the folding of the pmoA peptide are anticipated, it should be noted that each of the copper binding peptide in the SAMTEL polymer faces outward of the polymer backbone and is isolated thus allowing the peptide to behave as it would in solution. Moreover, the putative copper binding pmoA peptide is at the end of an α-helix in the pMMO enzyme. Therefore, fusing the peptide to the end of another α-helix of the SAMTEL monomer would only further facilitate the folding of the peptide as it would in its native form.

The benefits of employing this SAMTEL V80E polymerization module for the structure determination of the pmoA peptide extend farther than just as a crystallization tool. Since the structure of the SAMTEL V80E mutant has already been determined using X-ray crystallography, initial crystallization screening for the SAMTEL/pMMO fusion protein can focus on the conditions used to obtain the SAMTEL V80E mutant. Also, the structure determination of the SAMTEL/pMMO fusion protein is expedited since molecular replacement of the known SAMTEL structure can be utilized to account for

the majority of the electron density map generated by the diffraction data of the SAMTEL/pMMO fusion protein.

CHAPTER 3

METHODS

3.1 SAM1TEL-pmoA(38-49) FUSION PROTEIN

A. Cloning of SAM1TEL/pMMO

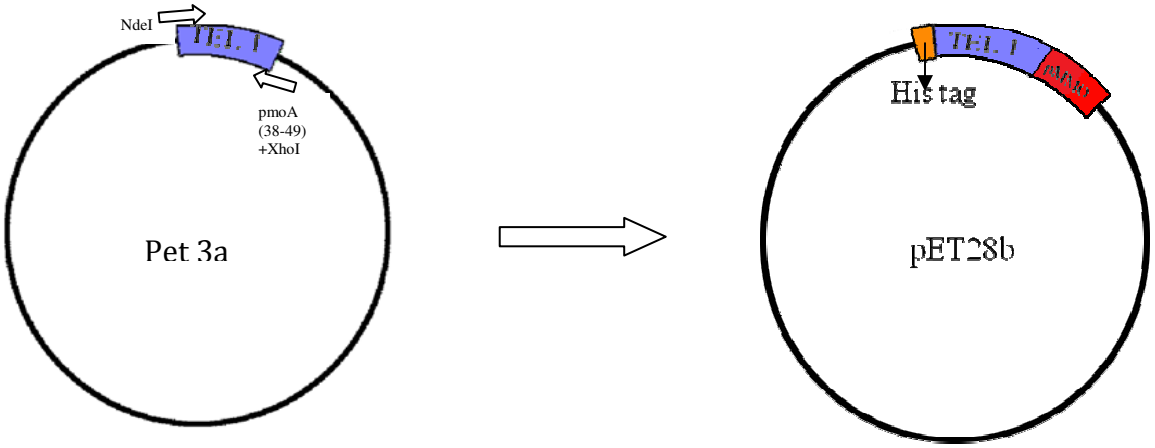

Fig. 3.1. Diagram displaying the cloning strategy used to obtain the SAM1TEL/pMMO pET28b vector

The SAM1TEL wild-type DNA in pET3a vector was kindly donated by the Bowie lab at UCLA. The pmoA (38-49) DNA sequence was fused to the 3' end of the SAM1TEL wild-type DNA by incorporating the pmoA(38-49) DNA sequence into the 3' primer along with an XhoI cut site. The 5' primer included an NdeI cut site. These cut sites were engineered into the primers for the purpose of cloning the SAM1TEL/pmoA construct obtained from PCR into the pET28b vector.

The SAM1TEL/pmoA construct with an approximate length of 300 DNA basepairs was verified by agarose gel electrophoresis. Following this, any exogenous

DNA from the PCR reaction was removed by PCR purification using Qiagen purification kit.

The SAM1TEL/pmoA DNA construct as well as the pET 28b with an N-terminal His tag were thendigestedusing NdeI and XhoI restriction enzymes. The restriction enzyme digested products were then run on a DNA agarose gel and the corresponding bands extracted according to the Qiagen gel extraction kit. The SAM1TEL/pmoA DNA construct was then ligated into the pET28b vector using T4 ligase. The SAM1TEL/pmoA pET 28b vector was transformed into XL-10 gold competent cells and plated onto LB plates containing 50 µg/mL kanamycin. Colonies were harvested to yield large quantities of the SAM1TEL/pmoA pET28b vector via miniprep using Qiagen miniprep kit. The SAM1TEL/pmoA construct DNA sequence was verified using DNA sequencing, which showed no unwanted DNA mutations.

The SAM1TEL/pmoA V80E mutant containing the necessary mutation for the pH dependent polymerization of the SAMTEL domain was obtained using site directed mutagenesis. Following site directed mutagenesis PCR reaction, DpnI was added to eliminate non-mutated methylated DNA. The final SAM1TEL/pMMO construct with the V80E mutation was verified using DNA sequencing.

B. SAM1TEL/pMMO protein expression

The SAM1TEL/pMMO plasmid was transformed into BL21(DE3)pLysR competent cells and plated onto LB plates containing 50 µg/mL kanamycin. One liter LB kanamycin (50 µg/mL) cultures were inoculated with 5 mL small cultures prepared from single colonies from the plate. The 1 L large culture was grown at 37 ºC and 250 rpm

until OD_{600} 0.6 when it was induced with 0.001 M IPTG and allowed to express the protein of interest for 4-5 h. The large culture cells were harvested via centrifugation at 4K rpm for 30 min and stored at -80 ºC until use.

C. SAM1TEL/pMMO protein purification

The cell pellet from expression was thawed at room temperature and resuspended in 20 mM Tris, pH 8.2, 200mM NaCl, 30 mM imidazole, pH 7.8. The resuspended cells were sonicated for 6 x 1 min at approximately 60 V with a 20 sec pause between successive sonications. The lysed cells were centrifuged at 18K rpm for 30 min and the supernatant was filtered using a 0.45 mm filter. The filtered supernatant was loaded into a 5-mL HisTrap column (GE Healthsciences) to undergo Nickel affinity chromatography. The SAM1TEL/pMMO fusion protein generally eluted at approximately 20 mM Tris, pH 8.2, 200 mM NaCl, 120 mM Imidazole. Peak fractions were run on a SDS-PAGE gel to analyze purity. SAM1TEL/pMMO fusion protein purity following nickel affinity chromatography was not optimal so anion exchange chromatography exploiting the pI of the fusion protein (4.90) was employed. Fractions containing SAM1TEL/pMMO fusion protein were pooled and diluted with 20 mM Tris pH 8.2 until imidazole and NaCl concentration totaled approximately 20 mM. The diluted protein fractions were then loaded in a 5-mL HPQ column (GE Healthsciences). The equilibration buffer consisted of 20 mM Tris pH 7.5, 25 mM NaCl and the elution buffer consisted of 20 mM Tris, pH 7.5, 1 M NaCl. The SAM1TEL/pMMO protein eluted at approximately 430 mM NaCl based on protein gel analysis of fractions. Pure protein fractions were then pooled and dialyzed into 20 mM Tris, pH 8.5, and 200 mM NaCl and concentrated to approximately

14 mg/mL using a Viaspin concentrator with MWCO 3000. The concentrated protein was run on a SDS-PAGE gel and the band of interest was excised and sent to a mass spec facility for protein I.D.

D. Crystallization of SAM1TEL/pMMO protein

The purified SAM1TEL-pMMO was used to set up hanging drop trays that induce crystal formation via the vapor diffusion method. SAM1TEL-pMMO protein crystals ranging from needles to hexagonal crystals were obtained using similar conditions to those used for the native SAMTEL protein: 1.6 M Li_2SO_4, 50 mM Tris-HCl pH 8.8, and 0.5 µL strontium chloride additive.

E. Structure determination of initial SAM1TEL/pMMO protein hexagonal crystals

The structure of the SAM1TEL/pMMO protein was solved by Dr. Marianne Lee using diffraction data collected at the Stanford Synchrotron Radiation Lightsource (SSRL).

F. Chemical characterization of SAM1TEL/pMMO protein

F.1 UV Titration

SAM1TEL/pMMO purified protein was digested with the appropriate amount of thrombin in order to cleave the his tag attached to the end of the fusion protein. Thrombin was added to the SAM1TEL/pMMO and allowed to incubate at 22 ºC for 20 h with gentle shaking. The histidine tag was removed prior to UV titration since it is capable of binding copper. 50 µM of SAM1TEL/pMMO deHis protein was titrated in increasing ratios of $Cu(OAc)_2$ to verify the ability of the pMMO peptide to bind copper. UV

absorbance was measured and recorded at 600 nm after each addition of $Cu(OAc)_2$ until the formation of heavy precipitate.

F.2. Extended X-ray absorption fine structure (EXAFS)

SAM1TEL/pMMO deHis protein was precipitated using 12 equivalents of $Cu(OAc)_2$ and sent to the Sunney Chan group (Academia Sinica, Taiwan) performed EXAFS experiment in order to analyze the copper binding ability of the fusion protein.

3.2 SAM1TEL-control PROTEIN

A. Obtaining SAM1TEL-control

The SAM1TEL-control was obtained by inserting the TAA stop codon before the pmoA DNA sequence using site-directed mutagenesis. DpnI was added to the SAM1TEL-TAA-pMMO control PCR product to remove non-mutated methylated DNA. The SAM1TEL-control DNA sequence was then transformed into DH5α competent cells and plated onto LB plates containing 50 µg/mL Kanamycin. Colonies were harvested to yield large quantities of the SAM1TEL-control pET28b vector via miniprep using Qiagen miniprep kit. The SAM1TEL-control verified using DNA sequencing.

B. SAM1TEL-control expression and purification

The SAM1TEL-control pET28b plasmid was transformed into BL21(DE3)pLysR competent cells and plated onto LB plates containing 50 µg/mL kanamycin. One liter cultures of 2x YT with kanamycin (100 µg/mL) were inoculated with 5 mL small

cultures prepared from single colonies from the plate. The 1 L large culture was grown at 37 ºC and 250 rpm until OD_{600} 0.6 when it was induced with 1 mM IPTG and allowed to express the protein of interest for 16 h. The large culture cells were harvested via centrifugation at 4K rpm for 30 min and stored at -80 ºC until use.

The cell pellet from expression was thawed at room temperature and resuspended in 20 mM Tris, pH 8.2, 200mM NaCl, 30 mM Imidazole, pH 7.8. The resuspended cells were sonicated for 7 x 1 min at approximately 60 V with a 20 sec pause between successive sonications. The lysed cells were centrifuged at 18K rpm for 30 min and the supernatant was filtered using a 0.45 mm filter. The filtered supernatant was loaded into a 5-mL HisTrap column (GE Healthsciences) to undergo Nickel affinity chromatography. The SAM1TEL-control protein eluted at approximately 20 mM Tris, pH 8.2, 25 mM NaCl, 150 mM imidazole. Peak fractions were run on a SDS-PAGE gel to analyze purity. The SAM1TEL-control purity following nickel affinity chromatography was not optimal so anion exchange chromatography exploiting the pI of the fusion protein (4.78) was employed. Fractions containing SAM1TEL-control protein was pooled and diluted with 20 mM Tris pH 8.2 until imidazole and NaCl concentration totaled approximately 20 mM. The diluted protein fractions were then loaded in a 5-mL HPQ column (GE Healthsciences). The equilibration buffer consisted of 20 mM Tris pH 7.5, 25 mM NaCl and the elution buffer consisted of 20 mM Tris, pH 7.5, 1 M NaCl. The SAM1TEL-control protein eluted at approximately 220 mM NaCl based on protein gel analysis of fractions. Pure protein fractions were then pooled and concentrated to approximately 14 mg/mL using an AMICON concentrator with MWCO 1000.

C. Chemical characterization of SAM1TEL-control

The N-terminal histidine tag of SAM1TEL-control was removed using thrombin digestion in order to prevent binding of copper to the his tag. Appropriate amounts of thrombin was added to SAM1TEL-control protein and incubated at 22 ºC for 20 hours with gentle shaking.

SAM1TEL-control deHis protein was precipitated using 12 equivalents of $Cu(OAc)_2$ and sent to Taiwan where the Sunney Chan group performed EXAFS experiment in order to analyze the copper binding ability of the fusion protein.

3.3 SAM3TEL-pmoA(38-49) FUSION PROTEIN

A. Cloning of SAM3TEL/pMMO

C1-AAGP SAM2TEL construct donated by the Bowie lab

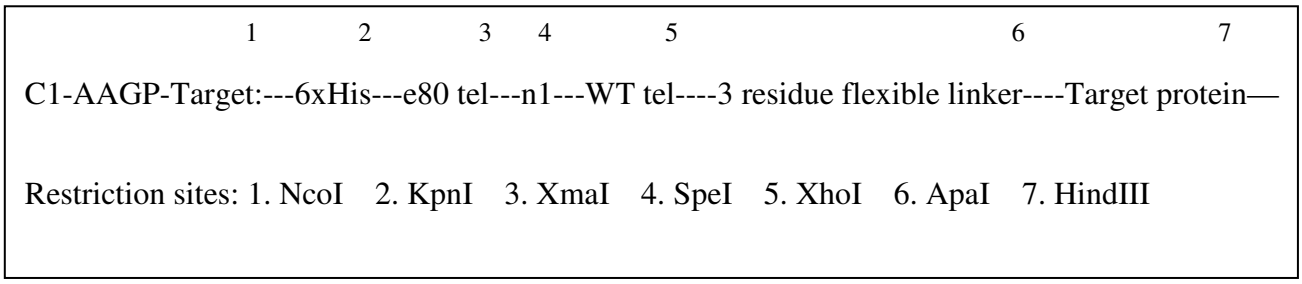

The SAM3TEL/pMMO protein was produced by excising the SAM1TEL/pMMO V800E mutant construct in pET28b and ligating it into the C1-AAGP construct shown above in pBAD-HisA vector (Invitrogen) between the ApaI and the HindIII cut sites. The

SAM1TEL/pMMO DNA construct was removed from the pET28b vector via PCR using primers containing the ApaI (in 5' primer) and the HindIII (in 3' primer) cut sites.

The SAM1TEL/pMMO V80E mutant fragment and the C1AAGP construct in pBAD-HisA were digested using sequential restriction enzyme digestion first with HindIII followed by ApaI. Both fragment and vector were then placed in a water bath at 65ºC for 20 min in order to deactivate the restriction enzymes. Following restriction enzyme digestion verification by DNA gel electrophoresis, the SAM1TEL/pMMO fragment and the C1AAGP in pBAD vector were ligated at a fragment: vector ratio of 6:1 using T4 ligase. The ligated product was transformed using DH5α competent cells and plated onto LB plate with ampicillin (100 µg/mL). Colonies were harvested to yield large quantities of the SAM3TEL/pmoA pBAD-HisA vector via miniprep using Qiagen miniprep kit. The SAM3TEL/pmoA DNA construct was sequenced to ensure no adverse mutations.

B. SAM3TEL/pMMO protein expression and purification

The SAM3TEL/pMMO pBAD plasmid was transformed into BL21(DE3)pLysR competent cells and plated onto LB plates containing 100 µg/mL ampicillin. One liter LB ampicillin (100 µg/mL) cultures were inoculated with 5 mL small cultures prepared from single colonies from the plate. The 1 L large culture was grown at 37 ºC and 250 rpm until OD_{600} 0.6 when it was induced with 0.02% of L-arabinose and allowed to express the protein of interest for 16 hours. The large culture cells were harvested via centrifugation at 4K rpm for 30 min and stored at -80 ºC until use.

The cell pellet from expression was thawed at room temperature and resuspended in 20 mM Tris, pH 8.6, 500mM NaCl, 30 mM imidazole, pH 7.8. The resuspended cells were sonicated for 7 x 1 min at approximately 60 V with a 20 sec pause between successive sonications. The lysed cells were centrifuged at 18K rpm for 30 min and the supernatant was filtered using a 0.45 mm filter. The filtered supernatant was loaded into a 5-mL HisTrap column (GE Healthsciences) to undergo nickel affinity chromatography. The SAM3TEL/pMMO fusion protein generally eluted at approximately 20 mM Tris, pH 8.6, 500 mM NaCl, 120 mM imidazole. Peak fractions were run on a 15% protein gel to analyze purity. SAM3TEL/pMMO fusion protein purity following nickel affinity chromatography was not optimal so anion exchange chromatography exploiting the pI of the fusion protein (6.90) was employed. Fractions containing SAM3TEL/pMMO fusion protein was pooled and diluted with 20 mM Tris pH 8.6 until imidazole and NaCl concentration totaled approximately 20 mM. The diluted protein fractions were then loaded in a 5-mL HPQ column (GE Healthsciences). The equilibration buffer consisted of 20 mM Tris pH 8.6, 25 mM NaCl and the elution buffer consisted of 20 mM Tris, pH 8.6, 1 M NaCl. The SAM3TEL/pMMO protein eluted at approximately 300 mM NaCl based on protein gel analysis of fractions. Pure protein fractions were then pooled and concentrated to approximately 6 mg/mL using an AMICON concentrator with MWCO 10,000.

C. Crystallization of SAM3TEL/pMMO fusion protein

The purified SAM3TEL-pmoA was used to set up hanging drop trays. Initial SAM3TEL-pmoA needle like protein crystals were obtained in 0.4 M Ammonium phosphate.

CHAPTER 4

RESULTS

4.1 SAM1TEL-pmoA(38-49) FUSION PROTEIN

A. Cloning of SAM1TEL/pMMO

The SAM1TEL-pmoA DNA construct was obtained, under the guidance of Dr. Marianne Lee, by incorporating the target pmoA sequence into a primer and amplifying by PCR in conjunction with SAMTEL domain in pET3a vector. The PCR results are shown in the DNA gel above. Lane a consists of the SAM1TEL-pmoA DNA construct, lane b is that of the SAM1TEL control without the pmoA DNA, and lane c is a control with simply the primers, PCR supermix, and DNA polymerase without any SAM1TEL pET3a vector. From the DNA gel, it can be seen that the SAM1TEL/pMMO PCR product is brighter and migrates slower than the SAM1TEL control as expected. We do not expect any product in lane c since it contained no plasmid for amplification.

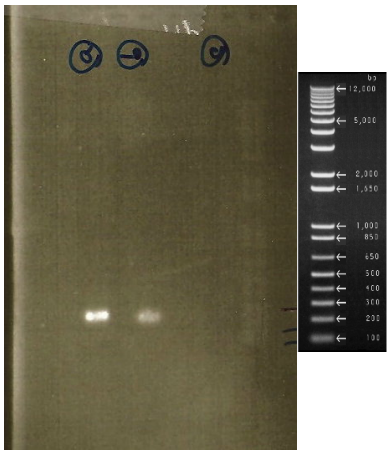

Fig. 4.1. Agarose [0.9% (w/v)] gel containing (a) SAM1TEL/pMMO DNA construct ~ 288 bp (b) SAM1TEL~252 bp (c) control-no SAM1TEL template

Once the SAM1TEL-pMMO PCR product was obtained, it was ligated into pET28b vector and transformed using XL10 gold competent cells via chemical transformation. Electroporation was also tested to transform the SAM1TEL/pMMO vector using DH5α. The SAM1TEL/pMMO pET28b vector obtained from the miniprep of the transformed cell culture was digested using restriction enzymes XhoI and NdeI and run on a DNA agarose gel.

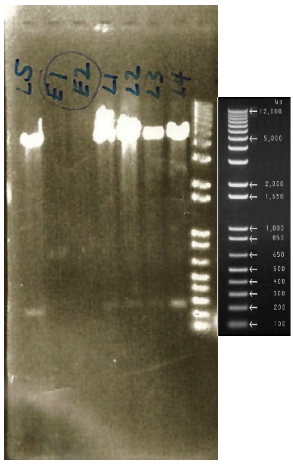

Fig. 4.2. Agarose [0.9% (w/v)] gel of Nde I and XhoI digested SAM1TEL/pMMO pET28b vector. L1-L5 correspond to SAM1TEL-pMMO pET28b from chemical transformation. E1-E2 correspond to transformation using electroporation

The restriction digestion was done precisely to verify that the SAM1TEL/pMMO construct was successfully incorporated into the pET28b vector. L1 through L5 are the chemical transformations using XL10 gold; their bands at around 5000 bp corresponding to the pET28b vector and at approximately 300 bp corresponding to the SAM1TEL/pMMO construct display the success of the transformation. The absence of bands in the E1 and E2 lanes suggest that electroporation using DH5α was not successful. The DNA from the chemical transformations were sequenced and verified to contain the proper SAM1TEL/pMMO DNA construct.

The necessary R20L and V80E mutations for pH dependent polymerization of the SAMTEL protein were incorporated into primers and executed using PCR. The methylated or non-mutated DNA in the PCR product was removed by the addition of DpnI. This can be seen in the DNA gel below where the PCR product before the addition of DpnI is brighter than the DNA product after DpnI. To verify the incorporation of the necessary mutations in the SAM1TEL/pMMO pET28b vector, the DpnI digested PCR product was transformed into DH5α competent cells. The miniprep yielded large quantities, 96 ng/µl, of the SAM1TEL/pMMO double mutant in pET28b (**Fig. 4.3** B), which were verified by DNA sequencing.

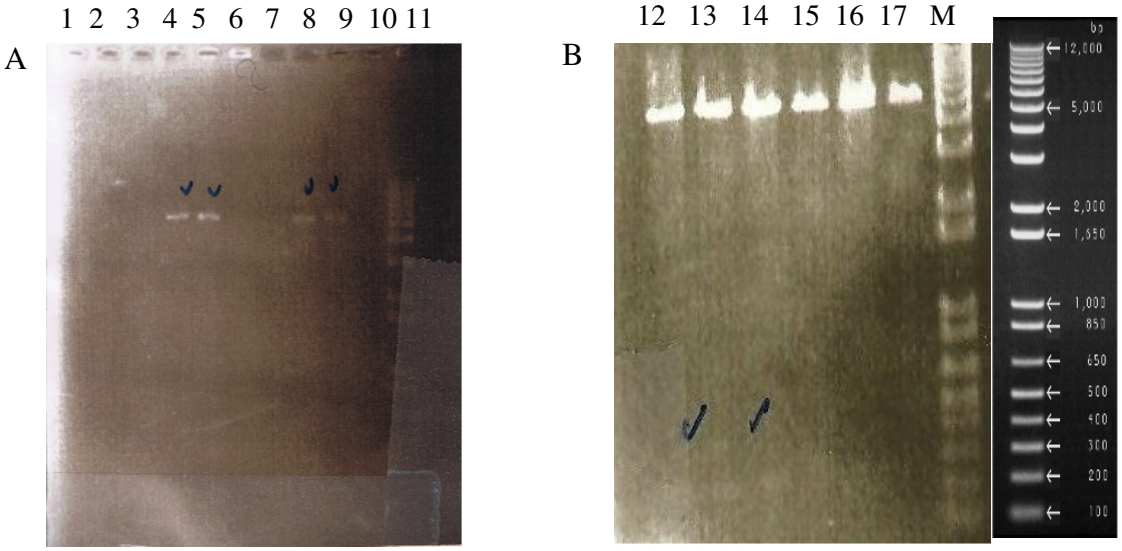

Fig. 4.3. (A) Agarose [0.9% (w/v)] gel showing PCR product following V80E site directed mutagenesis. Lanes 4-5 contains the SAM1TEL/pMMO pET28b mutated PCR product before the addition of DpnI. Lanes 8-9 contain the DpnI digested V80E SAM1TEL/pMMO pET28b. (B) Lanes 12-17 show miniprep results of V80E SAM1TEL/pMMO pET28b.

B. SAM1TEL/pMMO protein expression and purification

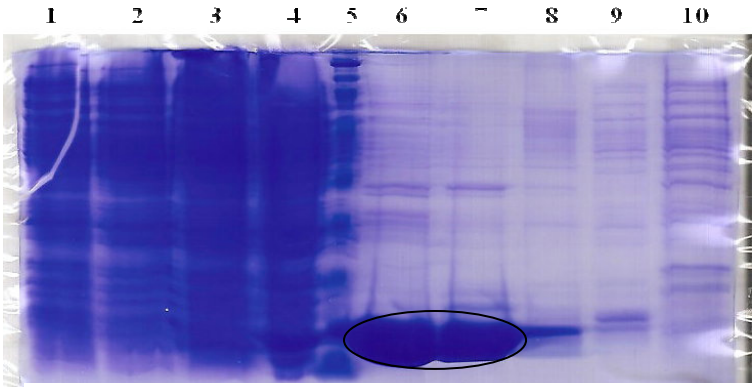

SAM1TEL/pMMO fusion protein

MW: 12771 kDa

Fig. 4.4. SDS-PAGE gel. Lanes 6-7 contain SAM1TEL/pMMO fusion protein following Ni^{2+} affinity chromatography

The SAM1TEL/pMMO was well expressed by *E.coli* as seen by the large quantity of fusion protein obtained in lanes 6 and 7 of the above gel. All gels were loaded with 15 µL of a 3 mL fraction and 3.5 µL of 5x SDS. The nickel affinity chromatography still left moderately strong bands at around 30 kDa and a few other weak protein bands. In order to obtain high purity SAM1TEL/pMMO fusion protein, fractions containing the SAM1TEL/pMMO protein were pooled, diluted to a low salt concentration, and loaded in 5mL HPQ anion exchange column. The protein gel below shows the high concentration and high level of purity of the SAM1TEL/pMMO fusion protein obtained.

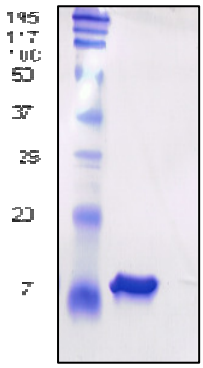

C.

Fig. 4.5. SDS-PAGE gel of SAM1TEL/pMMO protein following second purification using anion affinity chromatography

Crystallization of SAM1TEL/pMMO protein

Long rod shaped crystals or needle like crystals of SAM1TEL-pMMO were observed in initial growth of about one month in several crystallization conditions. Hexagonal crystals of SAM1TEL-pMMO protein were obtained in approximately two to three months in the following conditions: 1.6 M Li_2SO_4, 50 mM Tris-HCl pH 8.8, and 0.5 µL strontium chloride additive.

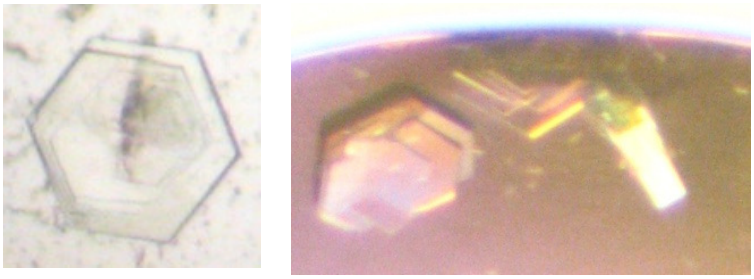

Fig. 4.6. SAM1TEL/pMMO fusion protein crystals

Blue crystals were obtained after direct addition of $Cu(OAc)_2$ to SAM1TEL/pMMO crystals and left to soak for several days. Analysis under fluorescence microscope revealed no fluorescence but we await X-ray diffraction data to make conclusions regarding the composition of these crystals.

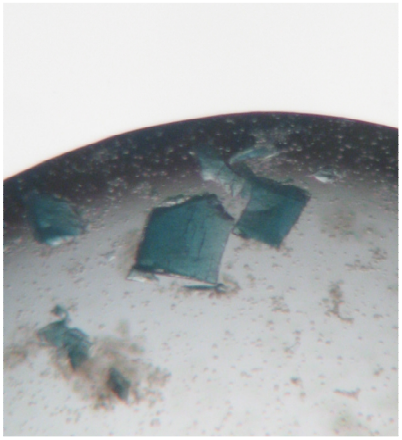

Fig. 4.7. Blue crystals found in SAM1TEL/pMMO crystallization condition after the addition of copper.

D. Structure Determination of SAM1TEL/pMMO

The SAM1TEL/pMMO hexagonal crystals resulted in a diffraction pattern to a resolution of approximately 2.8 Å. Structure determination based on the diffraction data using molecular replacement by Dr. Marianne Lee revealed that the SAM1TEL/pMMO fusion protein formed a tetramer.

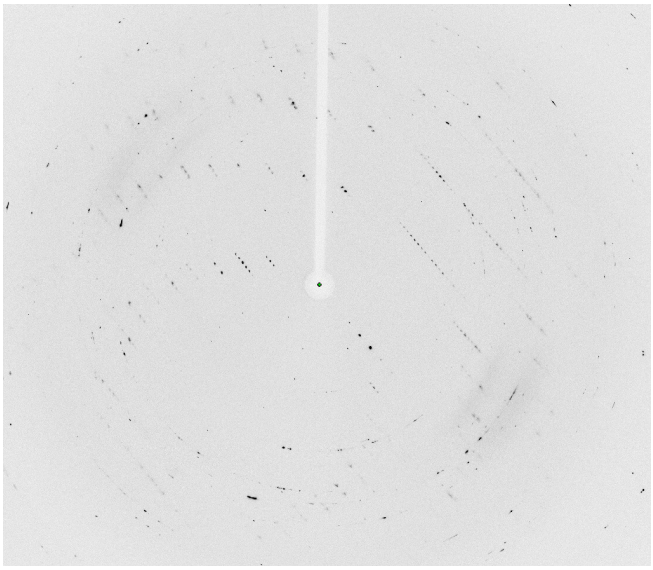

Fig. 4.8. SAM1TEL/pMMO hexagonal crystal diffraction data at a resolution of 2.8 Å

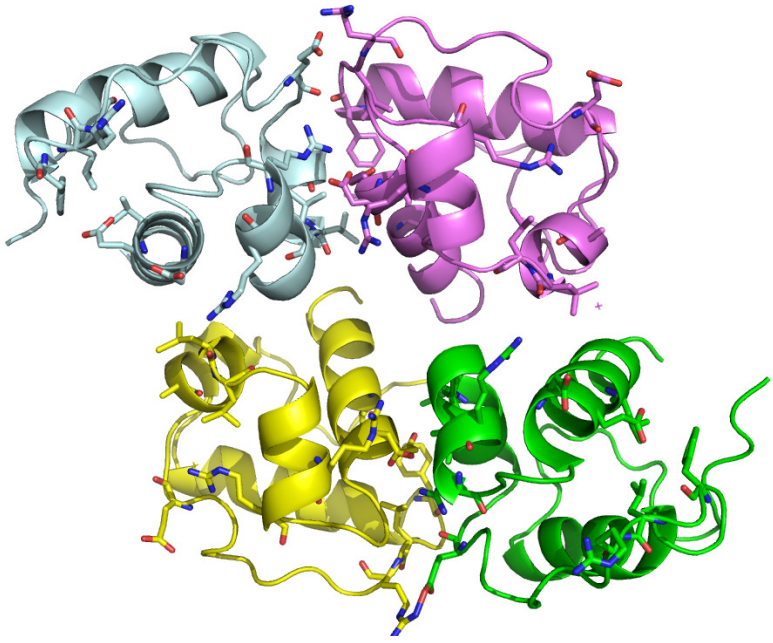

Fig. 4.9. SAM1TEL/pMMO crystal structure based on diffraction data at a resolution of 2.8 Å

E. Chemical characterization of SAM1TEL/pMMO protein

E.1. UV titration

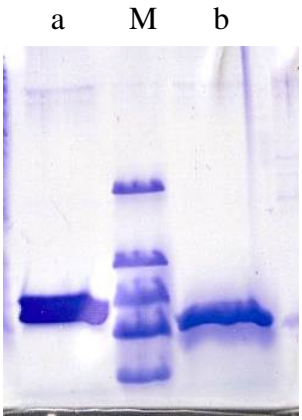

Fig 4.10. 15% protein gel displaying thrombin cleavage of 6x His Tag. Lane a contains SAM1TEL/pMMO before the addition of thrombin. Lane b is of SAM1TEL/pMMO following thrombin cleavage. The marker is a polypeptide marker.

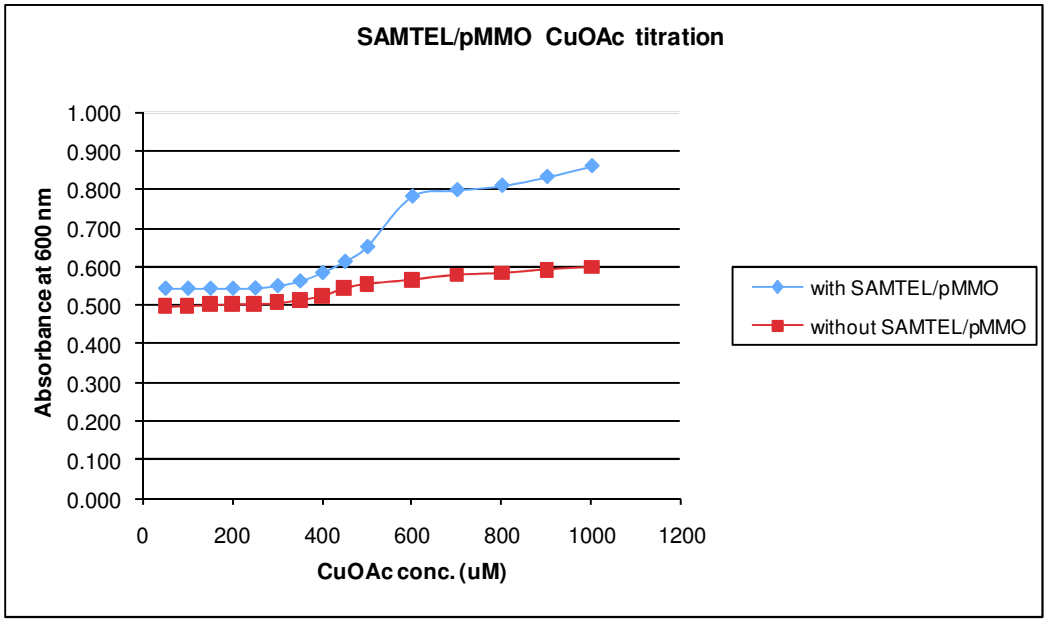

Fig. 4.11. Titration of SAM(TEL)-PmoA(38-49) with copper. The binding diagram is consistent with the formation of a cluster.

The UV titration of 50 µM SAM1TEL/pMMO deHis protein with increasing ratios of $Cu(OAc)_2$ displayed cooperative binding shown as a blue curve above at the characteristic absorbance of bound copper at 600 nm. As a control, the baseline red curve was produced with just the $Cu(OAc)_2$ without any SAM1TEL/pMMO protein.

E.2. Extended X-ray Absorption Fine Structure

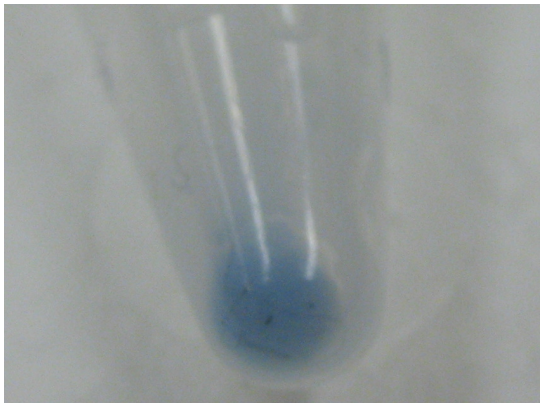

Fig. 4.12. SAM1TEL/pMMO + $Cu(Ac)_2$ precipitate

The SAM1TEL/pMMO fusion protein precipitated using 12 equivalents of $Cu(OAc)_2$. The blue color of the precipitate is worth noting since it visually supports the copper binding ability of the fusion protein.

Cu K-edge EXAFS Predictions		O, N	S	Cu
	Cu1	3	0	2
	Cu2	2	1	2
	Cu3	3	0	2
	Average	2.67	0.33	2

Best Fit

	CN	R(Å)
Cu-O	3	2.02(1)
Cu-S	0.3	2.52(2)
Cu-C	2	3.14(4)
Cu-Cu	2	3.49(1)

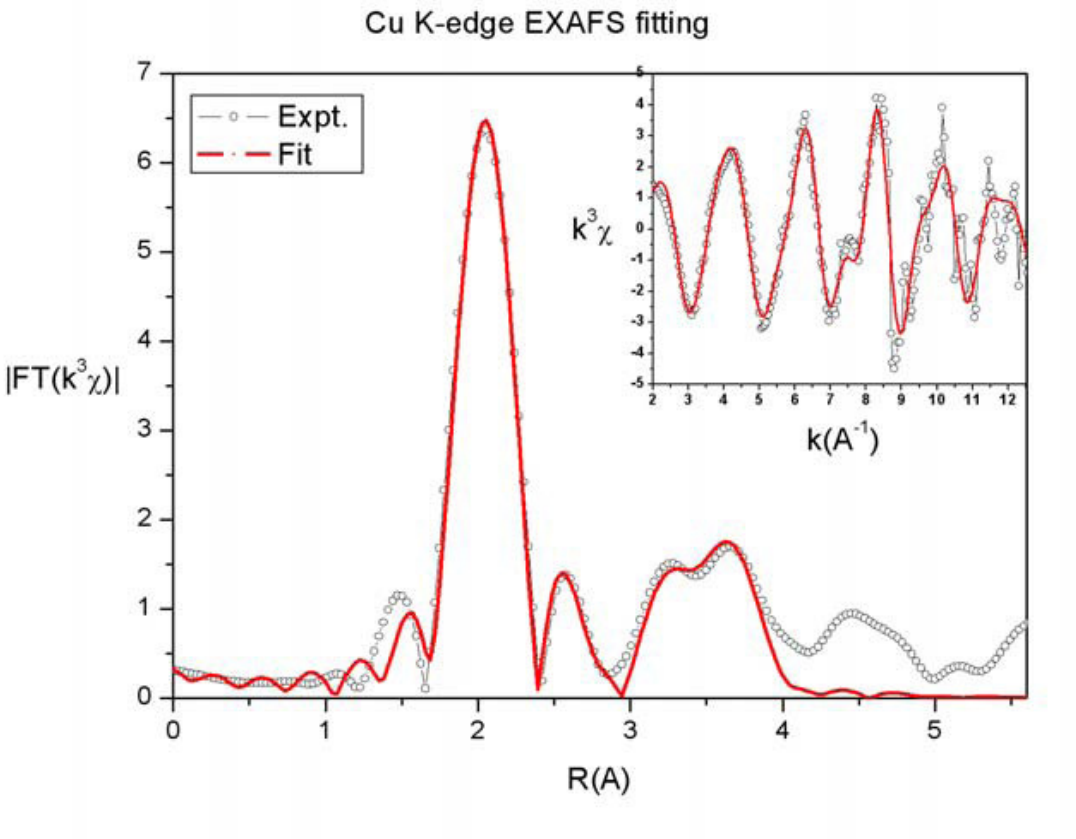

The EXAFS data of SAM1TEL/pMMO + $Cu(OAc)_2$ precipitate obtained by the S.I. Chan lab in Taiwan is shown above. The red line in the graph is the data pertaining to the theoretical trinuclear copper cluster and the grey dotted line is that of the SAM1TEL/pMMO fusion protein bound with copper. The experimental data fits quite well with the theoretical data of the trinuclear copper cluster. Moreover, the EXAFS data reveals that the SAM1TEL/pMMO fusion protein binds copper at a copper : peptide ratio of 3:1.

4.2 SAM1TEL-control PROTEIN

A. Obtaining SAM1TEL-control clone

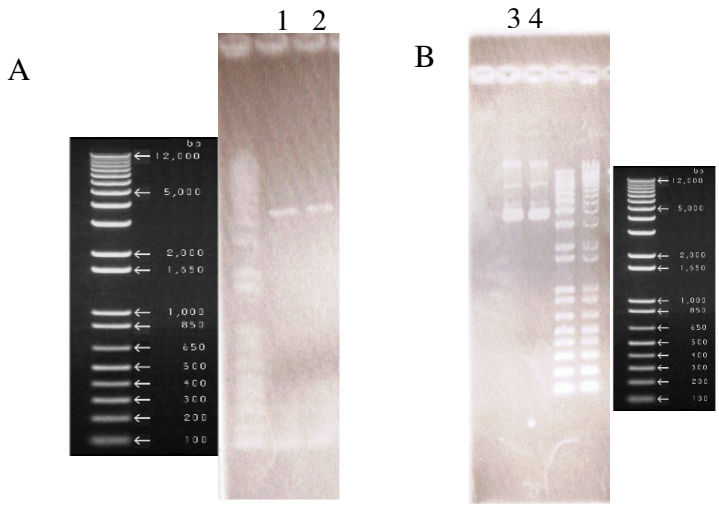

Fig. 4.13. (A) Agarose [0.9% (w/v)] gel showing PCR product following TAA insertion. Lane 1 shows the PCR product before DpnI. Lane 2 is the SAM1TEL-TAA-pMMO pET28b vector after DpnI. (B) Lanes 3 and 4 show the miniprep results of SAM1TEL-control

Fig. 4.13. (**A**) displays the DNA agarose gel of the PCR product following insertion of TAA stop codon between the SAM1TEL (V80E) mutant and the pmoA DNA sequence. The residual site directed mutagenesis primers were removed from the PCR product using Qiagen PCR purification Kit. The miniprep result from the small culture of transformed SAM1TEL-contol colonies are shown in lanes 3 and 4 of **Fig. 4.13.** (**B**). The insertion was verified by DNA sequencing.

B. SAM1TEL-control protein expression and purification

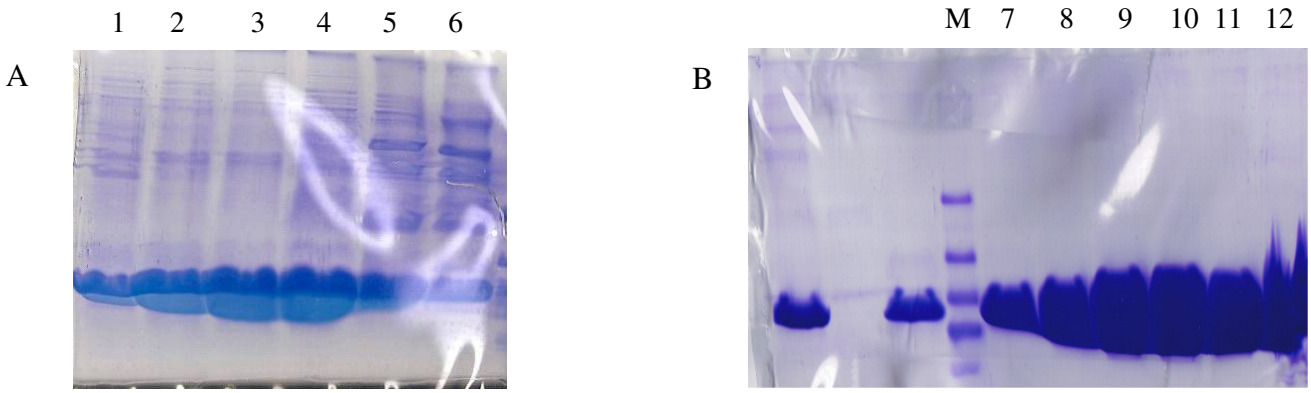

Fig. 4.14. 15% protein gel showing (A) SAM1TEL-control protein after Ni^{2+} affinity chromatography, and (B) Lanes 7-12 showing high yields of pure SAM1TEL-control following anion exchange chromatography.

The SAM1TEL-control expression results are similar to that of SAM1TEL/pMMO fusion protein. Large quantities of SAM1TEL-control were obtained as shown in lanes 1-6 **Fig. 4.14.** (A). All gels were loaded with 15 µL of a 3 mL fraction and 3.5 µL of 5x SDS. The nickel affinity chromatography still left several strong and weak protein bands. In order to further purify the SAM1TEL-control protein, fractions containing the SAM1TEL/pMMO protein (in lanes 1-6) were pooled, diluted to a low salt concentration, and loaded in 5mL HPQ anion exchange column. The protein gel in **Fig 4.14.** (B) shows the very high concentration and high level of purity of the SAM1TEL/pMMO fusion protein obtained. All lanes in **Fig. 4.14**. (B) contain 15 µL of a 3 mL fraction and 3.5 µL of 5x SDS

C. Chemical Characterization of SAM1TEL-control

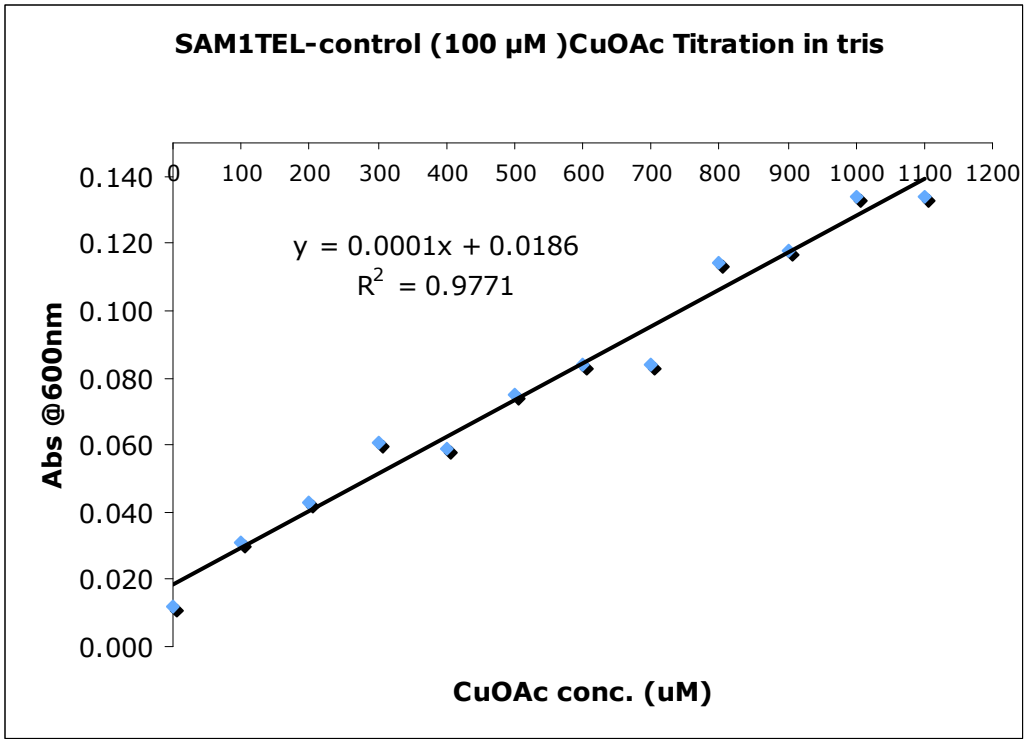

Fig. 4.15. UV titration of 100 µM SAM1TEL-control in Tris with increasing ratios of $Cu(OAc)_2$

The UV titration of 100 µM SAM1TEL-control with increasing ratios of $Cu(OAc)_2$ displayed a linear curve with low absorbance values at 600 nm.

4.3 SAM3TEL-pmoA(38-49) FUSION PROTEIN

A. Cloning of SAM3TEL/pMMO

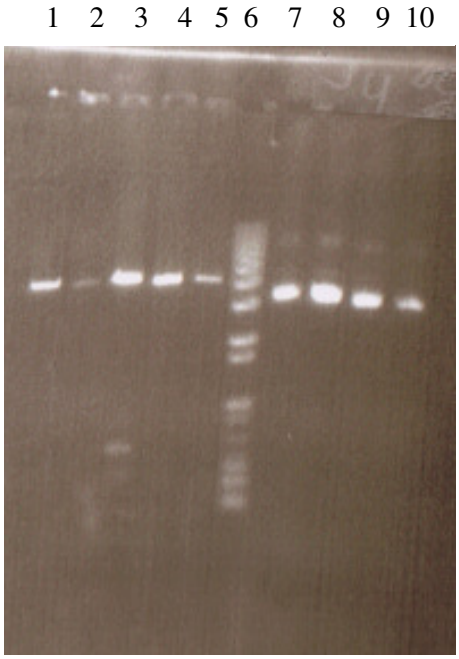

Fig. 4.16. Lanes 1-5, Agarose [0.9% (w/v)] gel of restriction digested SAM3TEL/pMMO. Lanes 7-10 are miniprep results of C1-AAGP SAM2TEL in pBAD-HisA vector

Lanes 1-5 in **Fig. 4.16**. is the DNA gel electrophoresis of restriction digested SAM3TEL/pMMO in pBAD-HisA vector. Restriction digestion was carried out with HindIII and ApaI, which cuts the SAM1TEL/pMMO construct from the SAM2TEL C1-AAGP in pBAD-HisA vector. The approximately 5000 bp band corresponds to the SAM2TEL pBAD-HisA vector while the approximately 300 bp band in lane 3 pertains to the SAM1TEL/pMMO construct. Lanes 7-10 are the circularized C1AAGP construct in pBAD-HisA. DNA sequencing confirmed that the product in lane 3 was that of SAM3TEL/pMMO.

B. SAM3TEL/pMMO protein expression and purification

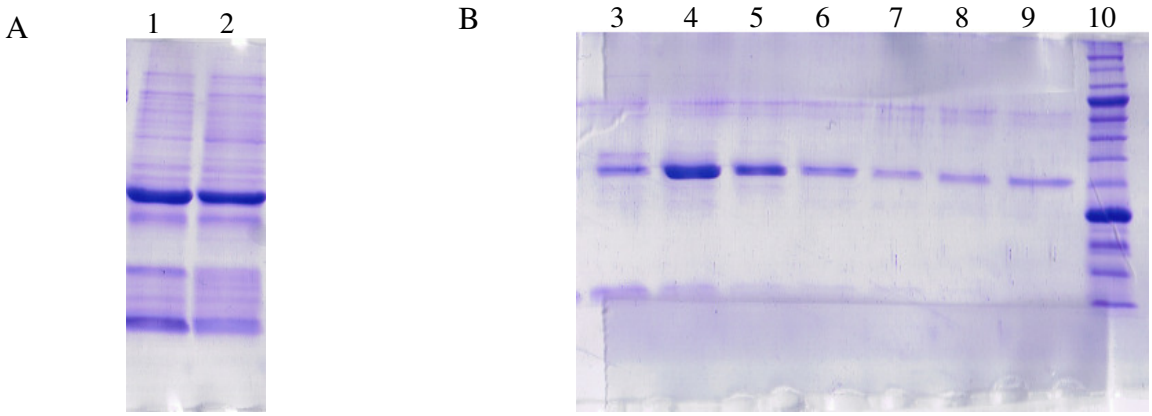

Fig. 4.17. 15% protein gel showing (A) Lanes 1and 2: SAM3TEL/pMMO protein after Ni^{2+} affinity chromatography, and (B) Lanes 7-12 showing low yields of slightly impure SAM3TEL/pMMO protein following anion exchange chromatography.

SAM3TEL/pMMO protein did not express in high amounts and the Ni^{2+} affinity chromatography resulted in low purity SAM3TEL/pMMO protein. Anion exchange chromatography purification of pooled SAM3TEL/pMMO fractions resulted in slightly better purity as shown in **Fig. 4.17.** (B).

C. Crystallization of SAM1TEL/pMMO protein

Thin, rod shaped crystals or needle like crystals of SAM3TEL-pMMO were observed in initial growth of about one month in 0.4 M ammonium phosphate. These crystals were identified as protein crystals from the fluorescence while viewed under a fluorescent microscope.

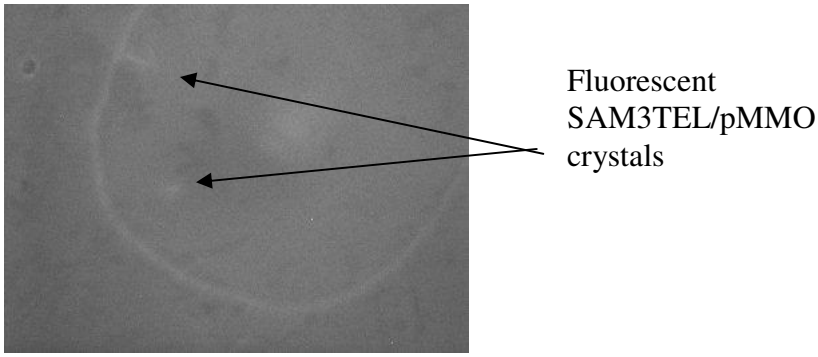

Fig. 4.18. SAM3TEL/pMMO as viewed in a fluorescence microscope. Dark regions signify protein crystals.

D. Chemical characterization of SAM1TEL/pMMO protein

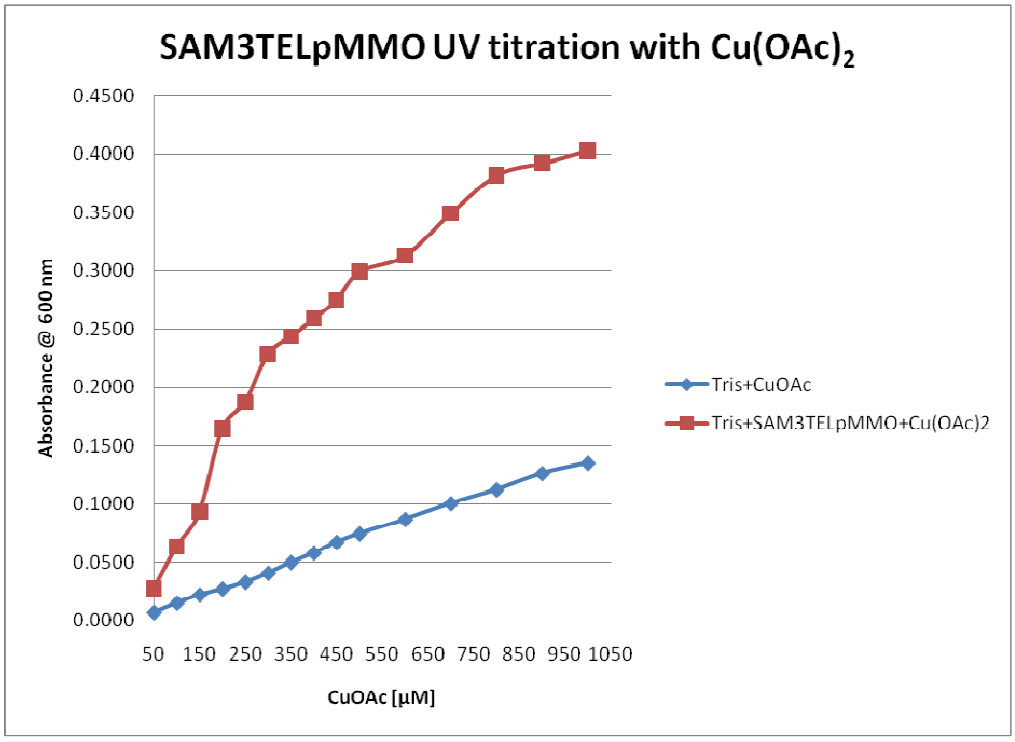

Fig. 4.19. UV titration of 11 µM SAM3TEL/pMMO in Tris buffer with increasing ratios of $Cu(OAc)_2$

The 11 µM SAM3TEL/pMMO protein was titrated in increasing ratios of $Cu(OAc)_2$ and the absorbance at 600nm of bound copper was recorded. The red curve above with increasing absorbance values shows that the SAM3TEL/pMMO + $Cu(OAc)_2$

is capable of binding copper. However, the low concentration of SAM3TEL/pMMO protein does not allow for any conclusions regarding the cooperative binding of the protein.

CHAPTER 5

Discussion

The main objective of this project is the structure determination of a pmoA(38-49) peptide from the membrane portion of the metalloenzyme known as particulate methane monooxygenase. Toward this objective, we successfully fused this small peptide to the C-terminus of a SAM1TEL protein with polymerization capabilities to facilitate crystallization. The SAM1TEL/pMMO fusion protein was well expressed by *E.coli* and large quantities of high purity protein was obtained following sequential purification methods; first exploiting the 6x histidine tag to purify using Ni^{2+} affinity chromatography and then anion exchange chromatography based on the isoelectric point of the fusion protein.

The SAM1TEL/pMMO protein was used to set up both hanging and sitting drop trays with Hampton screening kits and near the crystallization conditions used to obtain SAMTEL. Initial crystals of SAMTEL/pMMO after approximately two weeks were needle or rodlike resembling initial SAMTEL crystals. Hexagonal SAM1TEL/pMMO crystals characteristic of the 2TEL crystals were produced after 2-3 months in 1.6 M Li_2SO_4, 50 mM Tris-HCl pH 8.8, and 0.5 μL strontium chloride additive. The hexagonal crystal diffracted to a resolution of 2.8 Å. Unfortunately, upon analysis of the diffraction pattern by Dr. Marianne Lee, it was found that the SAM1TEL/pMMO protein had formed a tetramer rather than a polymer. The various SAM1TEL domains were thus found to be close together where the interactions between them could adversely affect the

folding of the pmoA peptide. A short portion of the pmoA peptide could be seen in the crystal structure but ideally, we wish to see the peptide in its entirety with bound copper ions.

To alleviate the complications with the SAM1TEL-pmoA protein, we pursued the crystallization of the SAM3TEL/pMMO fusion protein. The increase in the number of SAMTEL domains (3 vs. 1) would allow for proper polymerization of the protein thus preventing the unfavorable interactions noted in the SAM1TEL/pMMO tetramer. Fusing the pmoA peptide to every three SAMTEL domains would also increase space within the structure to allow for the independent folding of the pmoA peptide.

To produce the SAM3TEL/pMMO fusion protein, the previous SAM1TEL/pMMO DNA construct was removed and inserted into a SAM2TEL pBAD-HisA vector using restriction enzyme digestion and ligation. The SAM3TEL/pMMO protein expression is not ideal even after exploring other growth media such as 2x YT and Terrific Broth as an alternative to LB. The two-step purification involving metal affinity chromatography and anion exchange chromatography failed to yield high purity protein. In all purifications of SAM3TEL/pMMO, a band around 10 kDa persists. Any subsequent purification after the two step purification results in very low quantity of SAM3TEL/pMMO. Initial crystallization screening conditions produced needle like crystals in 0.4 M ammonium phosphate.

In order for the structure determination of both SAM1TEL/pMMO and SAM3TEL/pMMO protein to be pertinent, the hydroxylation activity of the pmoA peptide with copper must be retained, supporting the assertion of its role as an active site.

The activity of the pmoA peptide in the SAM1TEL/pMMO deHis fusion protein was tested using UV spectroscopy and measuring the characteristic absorbance of bound copper at 600 nm. SAM1TEL/pMMO protein was found to exhibit cooperative binding. More convincing data of the copper binding ability of the pmoA peptide came from EXAFS experiments conducted by the Sunney Chan lab in Taiwan. The experimental SAM1TEL/pMMO data matched that of the trinuclear copper cluster with a copper: peptide ratio of 3:1.

Chemical characterization of SAM3TEL/pMMO remains difficult due to the limited amount of protein available and due to the protein's less than optimal purity. UV titration of approximately 11 μM SAM3TEL/pMMO with $Cu(OAc)_2$ produced an increase in the absorbance at 600 nm due to bound copper. However, with such a small amount of protein, specific characteristics of the absorbance curve, such as cooperative binding, cannot be determined. The small quantity of SAM3TEL/pMMO protein obtained from each purification; usually less than 0.6 mg and its impurity prevents the characterization of SAM3TEL/pMMO using EPR and EXAFS experiments.

In order to accurately evaluate the UV titration and the EXAFS experiments conducted with SAM1TEL/pMMO, we produced the SAM1TEL-control protein to ensure that the SAMTEL domain does not bind copper and skew the data obtained. The UV titration of 100 μM SAM1TEL-control with $Cu(OAc)_2$ showed very low absorbance at 600 nm; even at 1100 μM of $Cu(OAc)_2$ or 11 times the amount of SAM1TEL-control protein, the absorbance only approached 0.14. The UV titration of SAM1TEL-control in Tris cannot be compared with the UV measurements of SAM1TEL/pMMO in Hepes

buffer + $Cu(OAc)_2$ since the two proteins existed in two different buffers. However, we can conclude from the low absorbance values and the linear absorbance curve of the UV titration of SAM1TEL-control that the copper binding ability of the protein is quite low.

Conclusion

We have successfully cloned, overexpressed, and crystallized both SAM1TEL/pMMO and SAM3TEL/pMMO fusion proteins. Pure SAM1TEL/pMMO fusion protein was obtained in high yields but SAM3TEL/pMMO has proven difficult to express and obtain with high purity. The expression conditions for SAM3TEL/pMMO must therefore be explored further in order to obtain a large amount of protein necessary for crystallization screening and chemical characterization.

Since the main objective of this research project is the structure determination of the pmoA peptide with bound copper ions, copper bound crystals must be obtained. SAM1TEL/pMMO protein crystals with the addition of small increments of $Cu(OAc)_2$ up to a final Cu^{2+} concentration of approximately 1 mM diffracted poorly. Recently, large blue SAM1TEL/pMMO protein crystals were obtained by Dr. Marianne Lee (Chan lab). Analysis of the SAM1TEL/pMMO blue crystals under the fluorescence microscope showed no fluorescence but diffraction data will be obtained in the future to verify the composition of these crystals.

Also, expanding on the recent chemical characterization experiments, the hydroxylation capability of the pmoA copper bound peptide should be investigated using previous procedures described in Chen *et al.* (2007) to test facile O-atom insertion into C-C and C-H bonds by trinuclear copper complexes. Gas Chromatography–Mass Spectrometry is one way to identify any hydroxylated compounds as a result of the activity of the pmoA peptide bound with copper ions.

WORKS CITED

1. Fossil Fuels. Institute for Energy Research. 2009. http://www.instituteforenergyresearch.org/energy-overview/fossil-fuels/

2. International Energy Annual 2006: World Energy Overview: 1996-2006. Energy Information Administration Official Energy Statistics from the U.S. Government. Dec. 2008 <http://www.eia.doe.gov/iea/overview.html?

3. Country Comparisons - Oil - Consumption. Central Intelligence Agency: The World Factbook. 9, Apr. 2009. https://www.cia.gov/library/publications/the-world-factbook/rankorder/2174rank.html

4. Mason, James and Bill Bailey. The Approaching World Oil Supply Crisis. Miller-McCune: Science and Environment, 22, Sept. 2008. http://www.miller-mccune.com/science_environment/the-approaching-world-oil-supply-crisis-714

5. The National Methane Hydrates R&D Program All About Hydrates. NETL: The Energy Lab. http://204.154.137.14/technologies/oil-gas/FutureSupply/MethaneHydrates/about-hydrates/about_hydrates.htm

6. Natural Gas Hydrates-Vast Resource, Uncertain Future. USGS: Science for a changing world. Fact Sheet FS-021-01. Mar. 2001. http://pubs.usgs.gov/fs/fs021-01/fs021-01.pdf

7. Klauda, J.B., and Sandler, S.I. (2005) Global Distribution of Methane Hydrate in Ocean Sediment, *Energy & Fuels* 19, 459-470.

8. Lee, S. and Holder, G.D. (2001) Methane hydrates potential as a future energy source, *Fuel processing technology* 71, 181-186.

9. World Proved Reserves of Oil and Natural Gas, Most Recent Estimates. Energy Information Administration Official Energy Statistics from the U.S. Government. 3, Mar. 2009. < http://www.eia.doe.gov/emeu/international/reserves.html>

10. Methanol Fuels Indy Race Cars and Cleaner Air. Methanol Institute. 21, May 1997. <http://www.methanol.org/altfuel/press/pr970521.html>

11. Clean Alternative Fuels: Methanol. U.S. Environmental Protection Agency. http://www.naftc.wvu.edu/NAFTC/data/factsheets/methfactsheetepa.pdf

12. US Patent 7288684 - Process for the direct production of methanol from methane. Patent Storm. 30, Oct. 2007. http://www.patentstorm.us/patents/7288684/fulltext.html

13. Hanson, R.S., and Hanson, T.E., (1996) Methanotrophic Bacteria, *Microbiological Reviews* 60, (2) 439-471.

14. Prior, S.D., and Dalton, H. (1985) The effect of copper ions on membrane content and methane monooxygenase activity in methanol-grown cells *Methylococcus capsulatus* (Bath), *J. Gen. Microbiol.* 131, 155-163.

15. Elango, N., Radhakrishnan, R., Froland, W.A., Wallar, B.J., Earhart, C.A., Lipscomb, J.D., and Ohlendorf, D.H. (1997) Crystal structure of the hydroxylase component of methane monooxygenase from Methylosinus trichosporium OB3b, *Protein Sci.* 6(3), 556-568.

16. Merkx, M., Kopp, D.A., Sazinsky, M. H., Blazyk, J. L., Muller, J., and Lippard, S. J. (2001) Dioxygen activation and methane hydroxylation by soluble methane monooxygenase: A tale of two irons and three proteins, *Angew. Chem., Int. Ed.* 40, 2782-2807.

17. Chan, S.I., Chen, K., Yu, S., Chen, C.L., Kuo, S. (2004) Toward Delineating the Structure and Function of the Particulate Methane Monooxygenase from Methanotrophic Bacteria, *Biochemistry* 43, 4421-4430.

18. Nguyen, H.-H. T., Elliott, S. J., Yip, J. H.-K., and Chan, S.I. (1998) The particulate methane monooxygenase from *Methylococcus capsulatus* (Bath) is a novel copper-containing t hree-subunit enzyme. Isolation and characterization, *J. Biol. Chem.* 273, 7957-7966.

19. Yu, S. S.-F., Wu, L.-Y., Chen, K. H.-C., Luo, W.-I., Huang, D.-S., and Chan, S. I. (2003) The stereospecific hydroxylation of [2,2-$^2H_2$] butane and chiral dideuteriobutanes by the particulate methane monooxygenase from *Methylococcus capsulatus* (Bath), *J. Biol. Chem.* 278, 14995-15005.

20. Lieberman, R.L. and Rosenzweig, A.C. (2005) Crystal Structure of a membrane-bound metalloenzyme that catalyses the biological oxidation of methane, *Nature* 434(7030), 177-182.

21. Balasubramanian, R., and Rosenzweig, A.C. (2007) Structural and mechanistic insights into methane oxidation by particulate methane monooxygenase, *Acc Chem Res.* 40(7), 573-580.

22. Yu, S. S.-F, Chen, K. H.-C., Tseng, M. Y.-H., Tseng, C.-F., Wang, Y.-S., Chen, Y.-J., Huang, D.-H., and Chan, S. I. (2003) Production of high-quality particulate methane monooxygenase in high yields from *Methylococcus capsulatus* (Bath) with a hollow-fiber membrane bioreaction, *J. Bacteriol.* 185, 5915-5924.

23. Xin, J. Y., Cui, J.R., Hu, X. X., Li, S. B., Xia, C. G., Zhu, L. M., and Wang, Y. Q. (2002) Particulate methane monooxygenase from *Methylosinus trichosporium* is a copper-containing enzyme, *Bio-chem. Biophys. Res. Commun.* 295, 182-186.

24. Chen, P. P.-Y., Chan, S. I. (2006) Theoretical modeling of the hydroxylation of methane as mediated by the particulate methane monooxygenase, *Journal of Inorganic Biochemistry*. 100, 801-809.

25. Chan, S. I., Wang V. C.-C., Lai, J. C.-H., Yu, S. S.-F., Chen, P. P.-Y., Chen, K. H.-C., Chen, C.-L., and Chan, M. K. (2007) Redox Potentiometry Studies of Particulate Methane Monooxygenase: Support for a Trinuclear Copper Cluster Active Site, *Angew. Chem. Int. Ed.* 46, 1992-1994.

26. Chan, S. I., Yu, and S. S.-F. (2008) Controlled Oxidation of Hydrocarbons by the Membrane-Bound Methane Monooxygenase: The Case for a Tricopper Cluster, *Acc. Chem. Res.,* 41(8), 969-979.

27. Chen, P. P.-Y., Yang, R. B.-G., Lee, J. C.-M., and Chan, S. I. (2007) Facile O-atom insertion into C-C and C-H bonds by a trinuclear copper complex designed to harness a singlet oxene. *PNAS*, 104(37), 14570-14575.

28. Tran, H. H., Kim, C. A., Faham, S., Siddall, M. C., and Bowie, J. U. (2002) Native interface of the SAM domain polymer of TEL, *BMC Struct. Biol.* 2:5.

29. Nauli, S., Farr, S., Lee, Y. J., Kim, H. Y., Faham, S., and Bowie, J. U. (2007) Polymer-driven crystallization, *Protein Sci.*, 16(11), 2542-2551.

30. Olah, G.A., A. Goeppert, and G.K.S. Prakash, Beyond oil and gas: The methanol economy. 2006, *Weinheim: Wiley-VCH*. 304.